



**CHALMERS**  
UNIVERSITY OF TECHNOLOGY

## **SQUIDs in biomagnetism: A roadmap towards improved healthcare**

Downloaded from: <https://research.chalmers.se>, 2024-03-20 11:00 UTC

Citation for the original published paper (version of record):

Körber, R., Storm, J., Seton, H. et al (2016). SQUIDs in biomagnetism: A roadmap towards improved healthcare. *Superconductor Science and Technology*, 29(11): Art. no. 113001-.  
<http://dx.doi.org/10.1088/0953-2048/29/11/113001>

N.B. When citing this work, cite the original published paper.

ROADMAP • OPEN ACCESS

## SQUIDs in biomagnetism: a roadmap towards improved healthcare

To cite this article: Rainer Körber *et al* 2016 *Supercond. Sci. Technol.* **29** 113001

View the [article online](#) for updates and enhancements.

### You may also like

- [Review of 2D superconductivity: the ultimate case of epitaxial monolayers](#)  
Christophe Brun, Tristan Cren and Dimitri Roditchev
- [A review of finite size effects in quasi-zero dimensional superconductors](#)  
Sangita Bose and Pushan Ayyub
- [Molecular attraction of condensed bodies](#)  
B V Derjaguin, I I Abrikosova and E M Lifshitz

## Roadmap

# SQUIDs in biomagnetism: a roadmap towards improved healthcare

Rainer Körber<sup>1</sup>, Jan-Hendrik Storm<sup>1</sup>, Hugh Seton<sup>2</sup>, Jyrki P Mäkelä<sup>3</sup>,  
Ritva Paetau<sup>3</sup>, Lauri Parkkonen<sup>4</sup>, Christoph Pfeiffer<sup>5</sup>, Bushra Riaz<sup>6</sup>,  
Justin F Schneiderman<sup>6</sup>, Hui Dong<sup>7,8,9</sup>, Seong-min Hwang<sup>7,10</sup>,  
Lixing You<sup>7,8,9</sup>, Ben Inglis<sup>11</sup>, John Clarke<sup>7,18</sup>, Michelle A Espy<sup>12</sup>,  
Risto J Ilmoniemi<sup>4,18</sup>, Per E Magnelind<sup>13</sup>, Andrei N Matlashov<sup>13</sup>,  
Jaakko O Nieminen<sup>4</sup>, Petr L Volegov<sup>13</sup>, Koos C J Zevenhoven<sup>4</sup>,  
Nora Höfner<sup>1</sup>, Martin Burghoff<sup>1</sup>, Keiji Enpuku<sup>14</sup>, S Y Yang<sup>15</sup>,  
Jen-Jei Chieh<sup>16</sup>, Jukka Knuutila<sup>17</sup>, Petteri Laine<sup>17</sup> and Jukka Nenonen<sup>17</sup>

<sup>1</sup>Physikalisch-Technische Bundesanstalt (PTB), Abbestraße 2-12, 10587 Berlin, Germany

<sup>2</sup>University of Aberdeen, Foresterhill, Aberdeen, AB25 2ZD, UK

<sup>3</sup>BioMag Laboratory, HUS Medical Imaging Center, University of Helsinki and Helsinki University Hospital, PO Box 340, FI-00029 HUS Finland

<sup>4</sup>Department of Neuroscience and Biomedical Engineering, Aalto University School of Science, PO Box 12200, FI-00076 Aalto, Finland

<sup>5</sup>Department of Microtechnology and Nanoscience - MC2, Chalmers University of Technology, SE-412 96 Gothenburg, Sweden

<sup>6</sup>MedTech West and the Institute of Neuroscience and Physiology, University of Gothenburg, Sweden

<sup>7</sup>Department of Physics, University of California, Berkeley, CA 94720, USA

<sup>8</sup>State Key Laboratory of Functional Materials for Informatics, Shanghai Institute of Microsystem and Information Technology, Chinese Academy of Sciences, Shanghai 200050, People's Republic of China

<sup>9</sup>CAS Center for Excellence in Superconducting Electronics (CENSE), Shanghai 200050, People's Republic of China

<sup>10</sup>Center for Biosignals, Korea Research Institute for Standards and Science, Daejeon 34113, Korea

<sup>11</sup>Henry H Wheeler, Jr Brain Imaging Center, University of California, Berkeley, CA 94720, USA

<sup>12</sup>Non-Destructive Testing & Evaluation Group, Applied Engineering and Technology Division, PO Box 1663, MS-P915, Los Alamos National Laboratory, Los Alamos, NM 87545, USA

<sup>13</sup>Applied Modern Physics Group, Physics Division, PO Box 1663, MS-D454, Los Alamos National Laboratory, Los Alamos, NM 87545, USA

<sup>14</sup>Kyushu University, Fukuoka, Fukuoka Prefecture, Japan

<sup>15</sup>MagQu Co. Ltd., No.12, Ln. 538, Zhongzheng Rd., Xindian Dist., New Taipei City 231, 23141 Taiwan

<sup>16</sup>National Taiwan Normal University, No. 88, Section 4, Ting-Chou Rd, Taipei 116, Taiwan

<sup>17</sup>Elektta Oy, PO Box 34, FI-00531 Helsinki, Finland

E-mail: [rainer.koerber@ptb.de](mailto:rainer.koerber@ptb.de), [jyrki.makela@hus.fi](mailto:jyrki.makela@hus.fi), [justin.schneiderman@neuro.gu.se](mailto:justin.schneiderman@neuro.gu.se), [donghui@mail.sim.ac.cn](mailto:donghui@mail.sim.ac.cn), [koos.zevenhoven@aalto.fi](mailto:koos.zevenhoven@aalto.fi), [Nora.Hoefner@Ptb.de](mailto:Nora.Hoefner@Ptb.de), [enpuku@sc.kyushu-u.ac.jp](mailto:enpuku@sc.kyushu-u.ac.jp), [Jukka.Nenonen@elektta.com](mailto:Jukka.Nenonen@elektta.com), [risto.ilmoniemi@aalto.fi](mailto:risto.ilmoniemi@aalto.fi) (Risto J Ilmoniemi), [jclarke@berkeley.edu](mailto:jclarke@berkeley.edu) (John Clarke)

Received 7 March 2016


Accepted for publication 14 June 2016

Published 19 September 2016



CrossMark

<sup>18</sup> Guest Editors: John Clarke and Risto J Ilmoniemi.

 Original content from this work may be used under the terms of the [Creative Commons Attribution 3.0 licence](https://creativecommons.org/licenses/by/3.0/). Any further distribution of this work must maintain attribution to the author(s) and the title of the work, journal citation and DOI.

## Abstract

Globally, the demand for improved health care delivery while managing escalating costs is a major challenge. Measuring the biomagnetic fields that emanate from the human brain already impacts the treatment of epilepsy, brain tumours and other brain disorders. This roadmap explores how superconducting technologies are poised to impact health care. Biomagnetism is the study of magnetic fields of biological origin. Biomagnetic fields are typically very weak, often in the femtoTesla range, making their measurement challenging. The earliest *in vivo* human measurements were made with room-temperature coils. In 1963, Baule and McFee (1963 *Am. Heart J.* **55** 95–6) reported the magnetic field produced by electric currents in the heart ('magnetocardiography'), and in 1968, Cohen (1968 *Science* **161** 784–6) described the magnetic field generated by alpha-rhythm currents in the brain ('magnetoencephalography'). Subsequently, in 1970, Cohen *et al* (1970 *Appl. Phys. Lett.* **16** 278–80) reported the recording of a magnetocardiogram using a Superconducting QUantum Interference Device (SQUID). Just two years later, in 1972, Cohen (1972 *Science* **175** 664–6) described the use of a SQUID in magnetoencephalography. These last two papers set the scene for applications of SQUIDs in biomagnetism, the subject of this roadmap.

The SQUID is a combination of two fundamental properties of superconductors. The first is flux quantization—the fact that the magnetic flux  $\Phi$  in a closed superconducting loop is quantized in units of the magnetic flux quantum,  $\Phi_0 \equiv h/2e$ ,  $\approx 2.07 \times 10^{-15} \text{ Tm}^2$  (Deaver and Fairbank 1961 *Phys. Rev. Lett.* **7** 43–6, Doll R and Näbauer M 1961 *Phys. Rev. Lett.* **7** 51–2). Here,  $h$  is the Planck constant and  $e$  the elementary charge. The second property is the Josephson effect, predicted in 1962 by Josephson (1962 *Phys. Lett.* **1** 251–3) and observed by Anderson and Rowell (1963 *Phys. Rev. Lett.* **10** 230–2) in 1963. The Josephson junction consists of two weakly coupled superconductors separated by a tunnel barrier or other weak link. A tiny electric current is able to flow between the superconductors as a supercurrent, without developing a voltage across them. At currents above the 'critical current' (maximum supercurrent), however, a voltage is developed. In 1964, Jaklevic *et al* (1964 *Phys. Rev. Lett.* **12** 159–60) observed quantum interference between two Josephson junctions connected in series on a superconducting loop, giving birth to the dc SQUID. The essential property of the SQUID is that a steady increase in the magnetic flux threading the loop causes the critical current to oscillate with a period of one flux quantum. In today's SQUIDs, using conventional semiconductor readout electronics, one can typically detect a change in  $\Phi$  corresponding to  $10^{-6} \Phi_0$  in one second. Although early practical SQUIDs were usually made from bulk superconductors, for example, niobium or Pb-Sn solder blobs, today's devices are invariably made from thin superconducting films patterned with photolithography or even electron lithography. An extensive description of SQUIDs and their applications can be found in the *SQUID Handbooks* (Clarke and Braginski 2004 *Fundamentals and Technology of SQUIDs and SQUID Systems* vol I (Weinheim, Germany: Wiley-VCH), Clarke and Braginski 2006 *Applications of SQUIDs and SQUID Systems* vol II (Weinheim, Germany: Wiley-VCH)).

The roadmap begins (chapter 1) with a brief review of the state-of-the-art of SQUID-based magnetometers and gradiometers for biomagnetic measurements. The magnetic field noise referred to the pick-up loop is typically a few  $\text{fT Hz}^{-1/2}$ , often limited by noise in the metallized thermal insulation of the dewar rather than by intrinsic SQUID noise. The authors describe a pathway to achieve an intrinsic magnetic field noise as low as  $0.1 \text{ fT Hz}^{-1/2}$ , approximately the Nyquist noise of the human body. They also describe a technology to defeat dewar noise.

Chapter 2 reviews the neuroscientific and clinical use of magnetoencephalography (MEG), by far the most widespread application of biomagnetism with systems containing typically 300 sensors cooled to liquid-helium temperature, 4.2 K. Two important clinical applications are presurgical mapping of focal epilepsy and of eloquent cortex in brain-tumor patients. Reducing the sensor-to-brain separation and the system noise level would both improve spatial resolution. The very recent commercial innovation that replaces the need for frequent manual transfer of liquid helium with an automated system that collects and liquefies the gas and transfers the liquid to the dewar will make MEG systems more accessible.

A highly promising means of placing the sensors substantially closer to the scalp for MEG is to use high-transition-temperature (high- $T_c$ ) SQUID sensors and flux transformers (chapter 3). Operation of these devices at liquid-nitrogen temperature, 77 K, enables one to minimize or even omit metallic thermal insulation between the sensors and the dewar. Noise levels of a few  $\text{fT Hz}^{-1/2}$  have already been achieved, and lower values are likely. The dewars can be made relatively flexible,

and thus able to be placed close to the skull irrespective of the size of the head, potentially providing higher spatial resolution than liquid-helium based systems. The successful realization of a commercial high- $T_c$  MEG system would have a major commercial impact.

Chapter 4 introduces the concept of SQUID-based ultra-low-field magnetic resonance imaging (ULF MRI) operating at typically several kHz, some four orders of magnitude lower than conventional, clinical MRI machines. Potential advantages of ULF MRI include higher image contrast than for conventional MRI, enabling methodologies not currently available. Examples include screening for cancer without a contrast agent, imaging traumatic brain injury (TBI) and degenerative diseases such as Alzheimer's, and determining the elapsed time since a stroke. The major current problem with ULF MRI is that its signal-to-noise ratio (SNR) is low compared with high-field MRI. Realistic solutions to this problem are proposed, including implementing sensors with a noise level of  $0.1 \text{ fT Hz}^{-1/2}$ .

A logical and exciting prospect (chapter 5) is to combine MEG and ULF MRI into a single system in which both signal sources are detected with the same array of SQUIDs. A prototype system is described. The combination of MEG and ULF MRI allows one to obtain structural images of the head concurrently with the recording of brain activity. Since all MEG images require an MRI to determine source locations underlying the MEG signal, the combined modality would give a precise registration of the two images; the combination of MEG with high-field MRI can produce registration errors as large as 5 mm. The use of multiple sensors for ULF MRI increases both the SNR and the field of view.

Chapter 6 describes another potentially far-reaching application of ULF MRI, namely neuronal current imaging (NCI) of the brain. Currently available neuronal imaging techniques include MEG, which is fast but has relatively poor spatial resolution, perhaps 10 mm, and functional MRI (fMRI) which has a millimeter resolution but is slow, on the order of seconds, and furthermore does not directly measure neuronal signals. NCI combines the ability of direct measurement of MEG with the spatial precision of MRI. In essence, the magnetic fields generated by neural currents shift the frequency of the magnetic resonance signal at a location that is imaged by the three-dimensional magnetic field gradients that form the basis of MRI. The currently achieved sensitivity of NCI is not quite sufficient to realize its goal, but it is close. The realization of NCI would represent a revolution in functional brain imaging.

Improved techniques for immunoassay are always being sought, and chapter 7 introduces an entirely new topic, magnetic nanoparticles for immunoassay. These particles are bio-functionalized, for example with a specific antibody which binds to its corresponding antigen, if it is present. Any resulting changes in the properties of the nanoparticles are detected with a SQUID. For liquid-phase detection, there are three basic methods: AC susceptibility, magnetic relaxation and remanence measurement. These methods, which have been successfully implemented for both *in vivo* and *ex vivo* applications, are highly sensitive and, although further development is required, it appears highly likely that at least some of them will be commercialized.

Chapter 8 concludes the roadmap with an assessment of the commercial market for MEG systems. Despite the huge advances that have been realized since MEG was first introduced, the number of commercial systems deployed around the world remains small, around 250 units employing about 50 000 SQUIDs. The slow adoption of this technology is undoubtedly in part due to the high cost, not least because of the need to surround the entire system in an expensive magnetically shielded room. Nonetheless, the recent introduction of automatically refilling liquid-helium systems, the ongoing reduction in sensor noise, the potential availability of high- $T_c$  SQUID systems, the availability of new and better software and the combination of MEG with ULF MRI all have the potential to increase the market size in the not-so-distant future. In particular, there is a great and growing need for better noninvasive technologies to measure brain function. There are hundreds of millions of people in the world who suffer from brain disorders such as epilepsy, stroke, dementia or depression. The enormous cost to society of these diseases can be reduced by earlier and more accurate detection and diagnosis. Once the challenges outlined in this roadmap have been met and the outstanding problems have been solved, the potential demand for SQUID-based health technology can be expected to increase by ten- if not hundred-fold.

Keywords: biomagnetism, SQUID, MRI, ULF MRI, MEG, MEG-MRI, magnetic nanoparticles

(Some figures may appear in colour only in the online journal)

---

**Contents**

1. SQUIDs and measurement systems: ultimate noise level	5
2. MEG for neuroscience and clinical applications	8
3. High transition temperature SQUIDs for MEG	11
4. Ultra-Low-Field-MRI	14
5. MEG–MRI: multimodal approach for spatiotemporally accurate neuroimaging	17
6. Neuronal current imaging in the brain via ultra-low-field MRI	19
7. Magnetic nanoparticles for immunoassay	22
8. The commercial roadmap	25

## 1. SQUIDS and measurement systems: ultimate noise level

Rainer Körber<sup>1</sup>, Jan-Hendrik Storm<sup>1</sup>, Hugh Seton<sup>2</sup>

<sup>1</sup>Physikalisch-Technische Bundesanstalt (PTB), Abbestraße 2-12, 10587 Berlin, Germany

<sup>2</sup>University of Aberdeen, Foresterhill, Aberdeen, AB25 2ZD, UK

### Status

SQUIDS in biomagnetism are used to measure the magnetic fields generated by ionic currents within the brain by MEG or the heart by MCG non-invasively and without contact. The magnetic flux density noise  $S_B^{1/2}$  ( $S_B$  being the power spectral density of the noise) of modern commercial MEG systems using low critical-temperature (low- $T_c$ ) SQUIDS is commonly limited to  $\sim 2 \text{ fT Hz}^{-1/2}$  by Johnson noise in the radiation shield and the metallised multilayer insulation (MLI) of the liquid helium (LHe) dewar [12]. This is adequate for conventional MEG detecting frequencies of up to 100 Hz, but impairs the study of high frequency signals. For example,  $S_B^{1/2}$  of the resting brain drops to  $\sim 0.5 \text{ fT Hz}^{-1/2}$  at  $\sim 400 \text{ Hz}$  when measured over the somatosensory cortex (see figure 1). Using an ultra-low-noise SQUID system with  $0.5 \text{ fT Hz}^{-1/2}$  enabled the detection of high frequency signals up to 1 kHz by MEG [13].

SQUIDS are also used to reduce noise in low field MRI of the human body [14, 15]. One of the first SQUID-MRI systems used a fixed field of 10 mT and tuned SQUID detection [15], but since then research has concentrated on ULF MRI which first prepolarizes the volume of interest by a field of approximately 100 mT and then records the MR signal at a much lower field (usually tens to hundreds of  $\mu\text{T}$ ) with un-tuned SQUID detection [14]. Such systems are based on coupling a superconducting pick-up coil inductively to a SQUID and can be used for both MEG and ULF MRI [13, 16]. Potential benefits of ULF MRI include advancements in functional brain imaging by either combining MEG and ULF MRI into one instrument or by

performing NCI (cf chapter 6). Common to all those applications of ULF MRI is the relatively poor SNR. Currently, the SQUID with the lowest system noise features a  $S_B^{1/2}$  of  $\sim 0.5 \text{ fT Hz}^{-1/2}$  [13].

This chapter discusses approaches to reduce the various noise contributions. We show that a total noise of  $\sim 0.1 \text{ fT Hz}^{-1/2}$  presents an ambitious but achievable target. Such an improvement would enable the non-invasive study of spiking activity by MEG. For ULF MRI the spatial resolution would be enhanced and NCI should become possible.

### Current and future challenges

#### Noise sources common to MEG and ULF MRI

The ultimate noise level is of physiological origin and given by thermal noise generated by body tissue of conductivity  $\sigma$ . Using the approach from [17], one can show that the equivalent  $S_B^{1/2}$  is approximately independent of the coil diameter  $d$  for  $d/z < 16/\pi$  where  $z$  is the distance to a conducting half-plane. For  $d/z > 16/\pi$ ,  $S_B^{1/2}$  reduces if  $d$  is increased. For the realistic experimental configuration of a surface coil with  $d = 68 \text{ mm}$ ,  $z = 25 \text{ mm}$  and  $\sigma = 0.1 (\Omega\text{m})^{-1}$  applicable for 1 kHz, Myers *et al* [17] obtain  $0.03 \text{ fT Hz}^{-1/2}$  for the half-plane,  $0.025 \text{ fT Hz}^{-1/2}$  for the torso and  $0.012 \text{ fT Hz}^{-1/2}$  for the arm, as shown in the centre of figure 2.

Turning to the instrumental side, noise from conventional biomagnetic dewars is the main contribution. The vacuum spaces incorporate copper wire radiation shields and MLI made from aluminium-coated polyester film to limit helium boil-off to about  $1 \text{ L day}^{-1}$ . To reduce noise to a level suitable for ULF MRI and high frequency MEG signals, a new design was developed with a shield made from alumina, an electrically insulating but thermally conducting ceramic [18] and MLI made from a finely-woven polyester textile coated on each side with 25 nm of aluminium. The metallization is masked where threads cross to create  $10 \mu\text{m}$ -wide electrically isolated metallization regions, so the material

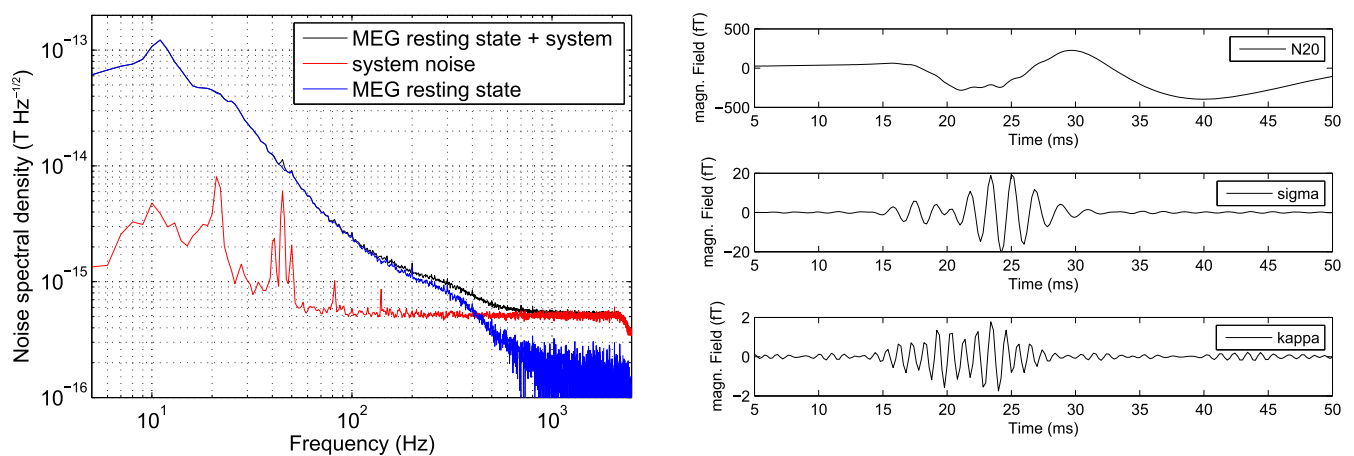


**Figure 1.** Left:  $S_B^{1/2}$  of the resting brain measured over the left somato-sensory cortex. Right: MEG-signal due to electro-stimulation of the median nerve. N20 component (full bandwidth), sigma-band (filtered: 450–750 Hz), kappa-band (filtered: 850–1200 Hz). Reproduced by permission from [13], copyright 2015 IOP Publishing.



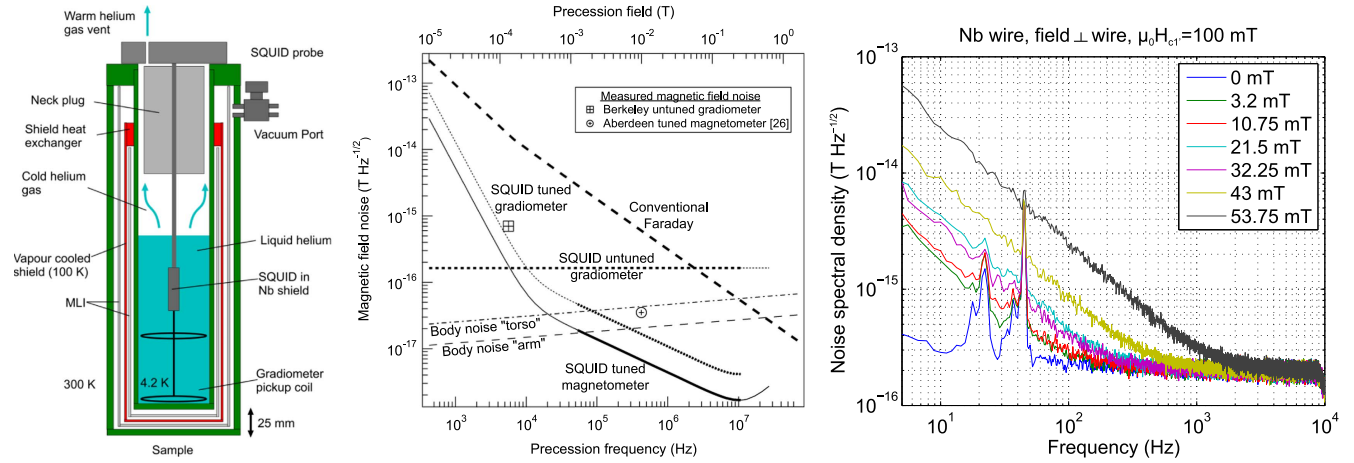


**Figure 2.** Left: Schematic ULF-MR SQUID setup with low-noise dewar. Centre: Calculated magnetic field noise of various detection schemes (Reproduced with permission from [17], copyright Elsevier). Right: Excess low frequency noise after pulsed fields (above  $H_{c1}$ , flux enters the wire).

has similar emissivity, but greatly reduced Johnson noise compared to standard MLI [18]. The noise contribution of this dewar was estimated to be  $0.035 \text{ fT Hz}^{-1/2}$  at 425 kHz [18] and the design achieves similar liquid helium boil-off rates to designs with conventional thermal insulation (see figure 2). This cryostat design was also used to reduce noise levels in ULF MRI with untuned SQUID detection.

MEG and ULF-MRI systems are usually operated in magnetically shielded rooms to suppress environmental field noise. However, the shield is also a noise source. Inside a mu-metal shield  $S_B^{1/2}$  was measured with SQUID magnetometers to be  $0.5 \text{ fT Hz}^{-1/2}$  at 100 Hz [19]. To reach lower  $S_B^{1/2}$  gradiometer pick-up coils can be used to reduce the noise contribution from the shield walls, provided the walls are further away than a few times the gradiometer baseline distance.

In order to discuss intrinsic SQUID noise contribution it is best to use the coupled noise energy per unit bandwidth  $\varepsilon_c$  as the figure of merit. It gives the equivalent energy of the minimal detectable current in the input circuit and takes into account both the intrinsic SQUID flux noise and the coupling of the SQUID to the input coil. In state-of-the-art low- $T_c$  SQUID current sensors,  $\varepsilon_c$  is about  $50 h$  ( $h$  Planck's constant) at 4.2 K. In order to avoid additional noise contributions from the read-out electronics, one can use a two-stage setup whereby a SQUID array is used as a cold amplifier. If a pick-up coil with area  $A_p$  and inductance  $L_p$  is connected to the SQUID, the equivalent field noise is given by  $S_B^{1/2} = (8\varepsilon_c L_p)^{1/2} / A_p$ . Hence, increasing the pick-up coil diameter  $d$  improves  $S_B^{1/2}$  and for a single turn pick-up coil one finds  $S_B^{1/2} \propto d^{-3/2}$ . As an example, assume a wire diameter of  $100 \mu\text{m}$ , no stray inductance and no coupling between gradiometer loops since this determines  $L_p$ : To achieve a  $S_B^{1/2}$  below  $0.1 \text{ fT Hz}^{-1/2}$  requires pick-up coil diameters  $d$  above 57 mm, 72 mm or 106 mm for a magnetometer, a 1st order gradiometer or a 2nd order gradiometer, respectively. For the gradiometer designs larger  $d$  are needed as the reference loops add only inductance to  $L_p$  without increasing the sensing area  $A_p$  for a given  $S_B^{1/2}$ . Such large coils are adequate for ULF MRI and also for MEG, provided integration of the inhomogeneous field over

the coil area in the forward model is carried out when solving the inverse problem. Overlapping the coils can then achieve the desired grid spacing to sample the spatial frequencies sufficiently. However, treating MRI/MEG signals as localised dipole sources at various depths places an upper limit on the diameter. In fact, for a given source depth an optimum diameter  $d_{\text{opt}}$  exists for which maximum signal flux is collected. For  $d > d_{\text{opt}}$  the field component detected by the coil has an opposite sign and the SNR decreases. Note, that this discussion requires the environmental noise to be negligible. If the noise is not limited by the SQUID it is actually better to use a large array of smaller diameter pick-up coils.

#### Noise sources unique to ULF MRI

The application of gradient fields, necessary for imaging, can lead to significant noise. In particular, if a readout-gradient is used, noise from the corresponding current source driving the gradient coil has to be suppressed as the concomitant gradient fields can couple, depending on geometry, into the pick-up coil. Assuming a typical readout gradient of  $100 \mu\text{T m}^{-1}$ , a current source with  $S_i^{1/2} / I_{\text{max}} = 10^{-9} \text{ Hz}^{-1/2}$  and a 100 mm baseline 1st order axial gradiometer results in a  $S_B^{1/2} \sim 5 \text{ fT Hz}^{-1/2}$ . For single-channel systems, this warrants the use of a 2nd order axial gradiometer and ultra-low-noise current sources to improve the noise to below  $0.1 \text{ fT Hz}^{-1/2}$ . For multi-channel devices, one could potentially use signal space projection (SSP) to remove such noise dimensions even if magnetometers are used [20].

Another noise source has become critical as the strength of the prepolarisation field used to boost the SNR has been increased. If during prepolarisation the pick-up-coil wire, usually made of the type-II superconductor niobium (Nb), experiences a field above its lower critical field  $H_{c1}$ , flux will be trapped. During the signal acquisition phase when the prepolarization field is removed, rearrangement of the vortices may cause flux jumps resulting in excess low-frequency noise [21, 22]. An example is shown on the right in figure 2.



### Advances in science and technology to meet challenges

We now turn to advances in science and technology necessary to overcome the most critical noise contributions. The field noise of an inductively coupled SQUID magnetometer or gradiometer could potentially be decreased by downsizing the Josephson junctions to the nanometre scale. This leads to a reduction in  $\varepsilon_c = 16k_B T(LC)^{1/2}/\alpha^2$  since the junction capacitance  $C$  can be strongly reduced [23]. The SQUID inductance  $L$  can also be decreased, but then it becomes difficult to retain the coupling constant  $\alpha$  between the SQUID and input coil close to unity. Finally, to achieve the smallest possible  $\varepsilon_c$ , it is also conceivable but less practical to reduce the thermal energy  $k_B T$  by cooling the SQUID below 4.2 K.

Regarding the issue of excess low-frequency noise seen after pulsed fields, Nb seems to be the best wire material as it has one of the highest  $H_{c1}$  in known type-II superconductors. There appears to be a large spread in the behavior of different Nb wire samples, indicating an unsolved material issue. A possible alternative might be the use of a type-I superconductor such as lead [24] or thermocycling the gradiometer wire as demonstrated by Matlashov *et al* [22].

### Concluding remarks

The total noise of SQUID systems can potentially be reduced to below  $0.1 \text{ fT Hz}^{-1/2}$ . Considering MEG with small gradiometer pick-up coils ( $d \sim 20 \text{ mm}$ ) demands a reduction in SQUID noise. This could be achieved by nanometre-sized junctions for which a reliable technology has still to be established. For ULF MRI, measurements show  $0.1 \text{ fT Hz}^{-1/2}$  is readily achieved using tuned systems above tens of kHz [18]. However, we believe there is more potential if ULF MRI is performed below this frequency range and/or combined with MEG, justifying our focus on un-tuned systems utilising pre-polarising pulses. The appearance of excess low frequency noise is most critical in this context and it remains to be seen whether this can be overcome. In terms of noise,  $0.1 \text{ fT Hz}^{-1/2}$  can be achieved by a 2nd order gradiometer with  $d \sim 106 \text{ mm}$  coupled to a state-of-the art SQUID ( $\varepsilon_c \sim 50 h$ ) and operated inside an ultra-low noise dewar. Improving  $\varepsilon_c$  to  $10 h$  would allow a reduction of  $d$  to  $\sim 60 \text{ mm}$  while also facilitating matching to the SQUID inductance. It should be noted that for optimum SNR the source parameters are equally important, so that ‘the larger the better’ is not necessarily true. With this in mind a hybrid system with coils of different sizes may represent the best option for practical applications.

## 2. MEG for neuroscience and clinical applications

Jyrki P. Mäkelä<sup>1</sup>, Ritva Paetau<sup>1</sup>, Lauri Parkkonen<sup>2</sup>

<sup>1</sup>BioMag Laboratory, HUS Medical Imaging Center, University of Helsinki and Helsinki University Hospital, PO Box 340, FI-00029 HUS, Finland

<sup>2</sup>Department of Neuroscience and Biomedical Engineering, Aalto University School of Science, PO Box 12200, FI-00076 Aalto, Finland

### Status

The first MEG recording was performed in 1968 as a proof-of-concept measurement depicting spontaneous occipital ‘alpha rhythm’ with a single-channel induction-coil magnetometer. The introduction of SQUIDs increased the sensitivity of MEG by orders of magnitude. Gradiometric sensors and high-performance magnetically shielded rooms further improved MEG’s ability to detect spontaneous brain activity as well as evoked fields time-locked to sensory stimuli. The first whole-scalp MEG instrument, realized in 1993, was a major breakthrough, enabling simultaneous recording of neuromagnetic fields over the entire scalp. The shortened recording times decreased signal variability caused by varying states of alertness (vigilance changes). Eloquent (functionally particularly important) cortical areas producing evoked fields, sources of brain oscillations and epileptiform activity could be detected within a single session, and the interaction of the hemispheres could be studied for the first time [25]. Since then, MEG research topics have evolved from studies on sensory processing to analysis of functional connectivity between brain regions and towards questions related to development from infancy to adulthood [26]. To date, presurgical evaluation of epileptiform spike generators in patients with intractable focal epilepsy (figure 4) and the identification of eloquent cortex in patients with brain tumors or vascular malformations have been generally accepted as indications of clinical MEG studies [27, 28]. Identification of epileptic networks with low-amplitude, high-frequency activity is still challenging.

Cognitive functions such as attention, working memory and sensory awareness arise from widespread cortical networks. The complete view of these processes will require understanding of anatomical, functional and effective connectivity within and between distinct brain areas. MEG, with its excellent temporal and decent spatial accuracy, will play an important role in studying these complex brain functions (see figure 3). In parallel, MEG will provide tools to improve diagnostics and treatment of neurological disorders where the functional disconnection may be evident before the onset of clinical symptoms. MEG is a useful tool to identify ‘signatures’ of altered neuronal functional connectivity that can distinguish pathological processes from normal cognition. MEG studies may provide unique information regarding the changes in brain function responsible for cognitive decline and it may offer tools to track disease progression and to monitor effects of treatment strategies.

### Current and future challenges

The spatial detail level of the fields measured by MEG depends on the distance of the sensors from the brain. Shortening this ‘viewing distance’ would improve the spatial resolution of MEG by enabling more detailed solutions to the ill-posed inverse problem of estimating neural sources from MEG signals. The development towards MEG sensors situated significantly closer to the scalp than the present SQUIDs is a highly desirable direction for MEG.

The main running expense of a MEG unit is liquid helium. A modern system requires about 80 litres of liquid helium every week. The increasing price and decreasing availability of liquid helium have generated concerns during recent years.

Studies of human brain development in infant subjects require particularly sensitive measurement techniques. Although MEG, compared to electroencephalography (EEG), is not significantly affected by open fontanelle and skull sutures, pediatric MEG is currently measured with a rigid sensor array designed for adult heads. Consequently, these instruments are far from optimal for pediatric studies as the large distance from the sensors to the head surface may preclude signal detection. Smaller sensor arrays have been designed for this purpose (e.g., [31]), but they naturally have a limited use for the general population.

The MEG sources are usually visualized on separately acquired structural MR images. The required co-registration of MEG and MRI is prone to errors. Thus, measuring both MEG and MRI with the same sensor array would be desirable as it would automatically provide a precise co-registration of the two methods. Accurate anatomical information could also be used to constrain MEG source reconstruction for enhanced localization accuracy.

Analysis of spontaneous MEG activity may provide unprecedented information about the function of healthy brains and produce novel biomarkers of brain dysfunction in individual patients. These analysis methods require high-quality signals, new experimental setups addressing variable vigilance levels, and sophisticated artefact-removal and movement-compensation methods [32] for complete realization of their value.

Although MEG has proven valuable in localizing epileptic foci and functional cortical areas, new clinical indications would be important for the field and for the MEG industry. To produce a convincing amount of data for new indications of MEG in the clinical realm, multicenter MEG studies using standardized recording parameters [33] are highly desirable. Such studies also require development of ‘signal biobanks’ to enable flexible data sharing for the best value of the recordings.

### Advances in science and technology to meet challenges

High- $T_c$  SQUIDs could be applied to MEG with much reduced thermal shielding and thus shorter distance from the brain compared to the current liquid-helium-cooled SQUIDs. However, the sensitivity of high- $T_c$  SQUIDs is still clearly

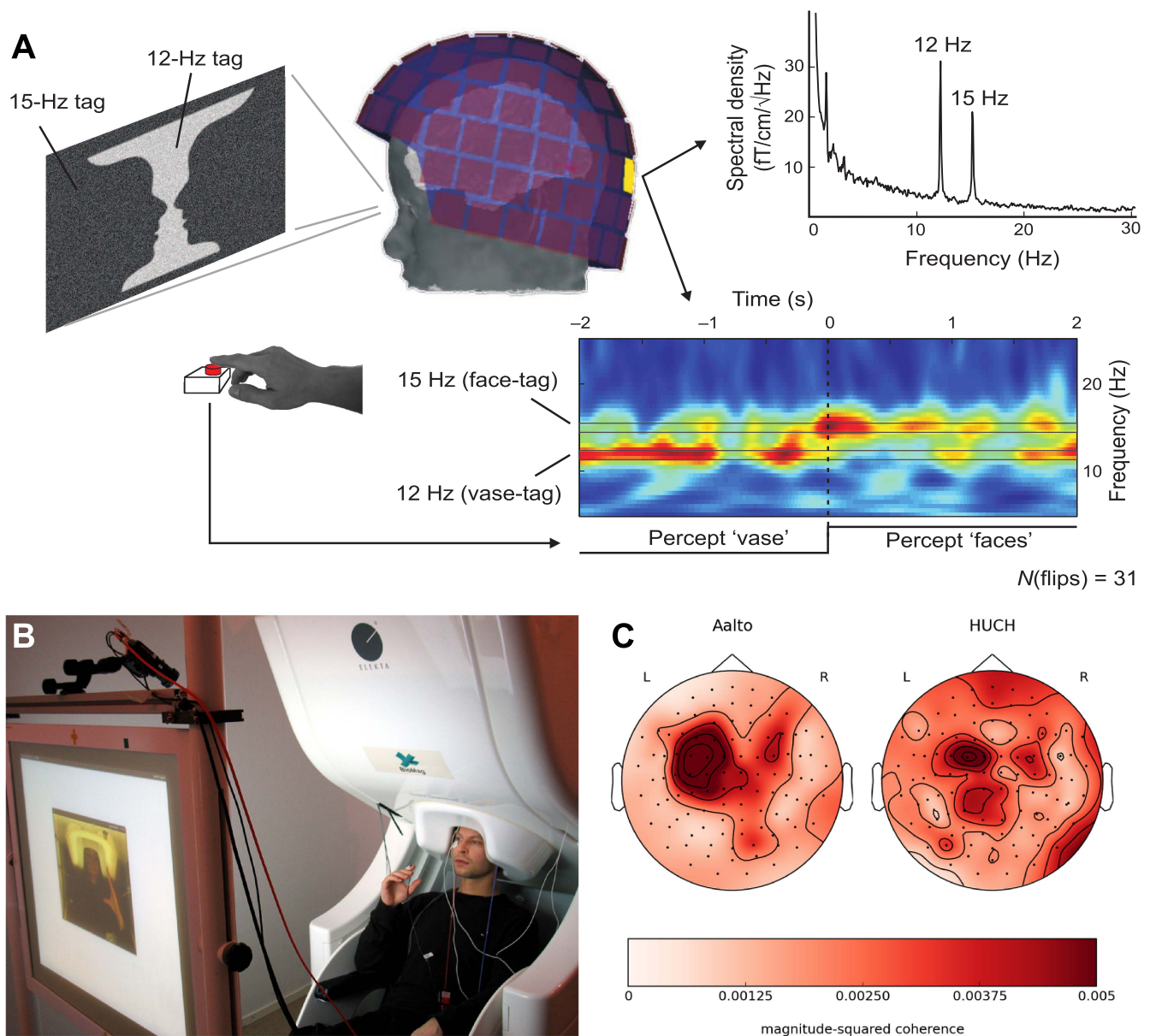


**Figure 3.** (A) MEG study of bistable visual perception using a frequency-tagged stimulus. Noise patterns refreshed at 12 and 15 Hz were superimposed on the vase-face figure and the subject was reporting the percept by a button press. MEG revealed that the representation of the area perceived as the foreground object is accentuated in the early visual cortices, manifested as an amplified tag signal. Reproduced with permission from [29], copyright 2008 Natl Acad. Sci.. (B) With a dual-MEG set-up, the brains of two interacting subjects can be measured simultaneously to study brain mechanisms supporting social interaction. Here the participants performed synchronous hand movements, which resulted in (C) coherent MEG signals from the motor cortices of the two participants. Reproduced with permission from [30], copyright 2015 PLOS.

inferior, and although the reduced distance to brain means larger signals, improvements in sensitivity are needed for high- $T_c$  SQUIDs to be on a par with their low- $T_c$  cousins, high- $T_c$  SQUIDs hold promise for an adjustable high-resolution MEG array [34].

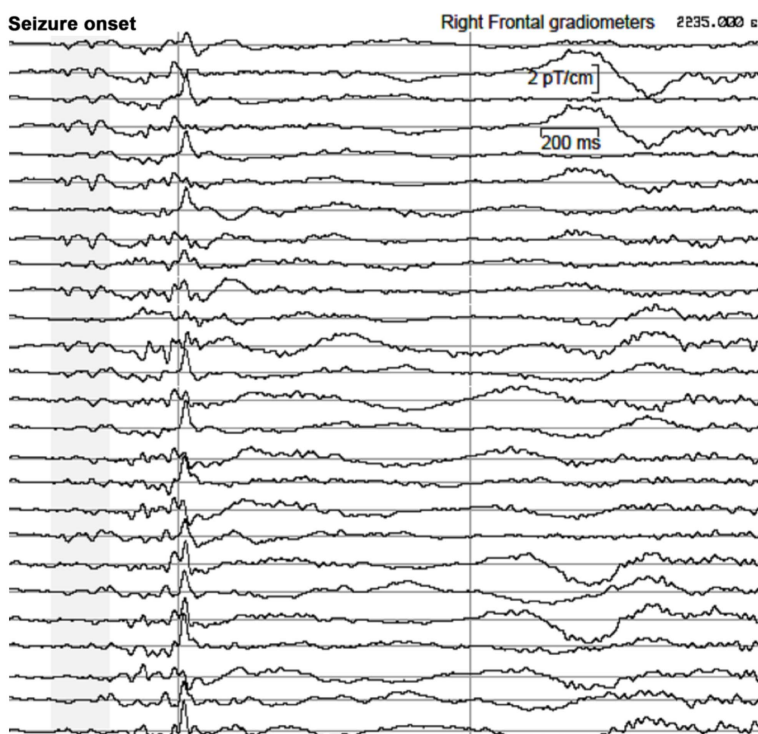
Optically-pumped magnetometers (OPM), based on magnetic-field-induced polarization rotation in an alkali-metal vapor, have demonstrated sensitivities approaching those of low- $T_c$  SQUIDs. MEG with chip-scale OPM sensors has been demonstrated [35]. Such sensors would enable construction of a multi-channel MEG system with an individually-adjustable array, where the sensors are within millimetres from the scalp.

Both high- $T_c$  SQUIDs and OPMs would remove the problems related to liquid helium. However, zero helium boil-off MEG systems have been introduced recently. This development clearly enhances the usability of MEG in hospitals, as the need for frequent transfers of liquid helium, requiring expertise and personnel, is eliminated (see chapter 8). Further development is required to lift the operating-time limitations due to the cryocoolers.

MEG systems designed particularly for neonatal brain assessment could solve problems related to low SNR. Systems based on high- $T_c$  SQUIDs or OPMs could potentially be made malleable to optimally fit also the heads of neonates and



## A. Seizure onset trace



## B. Seizure-onset dipole

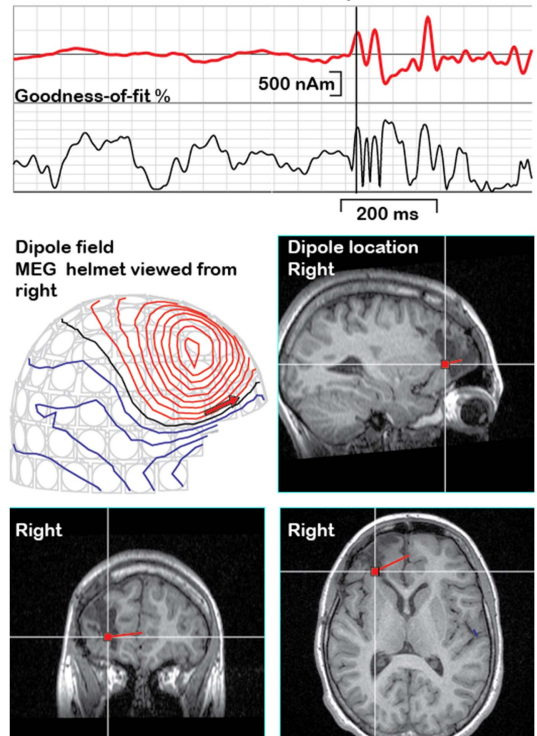


**Figure 4.** An example of an analysis of a large-amplitude epileptiform MEG signal. (A): Seizure-onset spikes from right frontal gradiometers. (B): A single dipole (red trace) explains 60%–70% of the field variation during the seizure onset spikes. This dipole guided the extension of unsuccessful earlier surgery, and the patient became seizure-free.

children, whereas a low- $T_c$  SQUID-based system needs to be specifically designed for such small heads.

Ultra-low-field MRI functionality could be added to existing MEG designs, assuming sufficient field tolerance of the SQUIDs, as a low-cost upgrade, without degrading the MEG quality of the system [36]. Such devices, enabling simultaneous measurement of MEG and MRI, would alleviate problems related to the alignment of functional and anatomical data. This development requires SQUIDs clearly more tolerant to magnetic fields than those already available.

Novel analysis methods revealing cortico–cortical functional connectivity patterns from spontaneous MEG activity and their implementation in open-source analysis packages would provide new possibilities in both basic research and clinical studies. New artefact suppression methods, such as removing the sensor-specific uncorrelated part of multi-channel MEG signals, will need to be developed further and made widely available. The clinical MEG community needs to form consortia and databanks for the most important,

unsolved clinical questions to make MEG truly useful in the most prevalent and costly neurological disorders.

## Concluding remarks

The emerging trend in MEG development strives to achieve recordings closer to the scalp. High- $T_c$  SQUIDs and optically-pumped magnetometers could realize this aim in the near future. This effort, in combination with the development of increasingly more sophisticated data analysis methods, will aid in unravelling the detailed neural coding related to perception and cognition, for example, to enable the read-out and identification of individual words directly from brain activity during single presentations, nowadays possible only from direct cortical recordings. In addition to epilepsy and functional mapping, new clinical indications are emerging for MEG. Several neurological and psychiatric diseases may be associated with an abnormal pattern of specific brain oscillations—the oscillopathies [37]—as well as with altered functional connectivity patterns. MEG, with its millisecond temporal resolution, is a valuable tool for revealing the intricacies of such pathologies.

### 3. High transition temperature SQUIDs for MEG

Christoph Pfeiffer<sup>1</sup>, Bushra Riaz<sup>2</sup> and Justin F Schneiderman<sup>2</sup>

<sup>1</sup>Department of Microtechnology and Nanoscience - MC2, Chalmers University of Technology, SE-412 96 Gothenburg, Sweden

<sup>2</sup>MedTech West and the Institute of Neuroscience and Physiology, University of Gothenburg, Sweden

#### Status

Today's MEG technology has enabled remarkable gains in our understanding of the human brain and our ability to treat it in disease [25]. Its development pushed an explosion in the market exploitation of superconducting technology: with hundreds of SQUIDs housed inside each system, MEG has been one of the main drivers of commercial SQUID research and development since the early 1990s. However, modern MEG hardware has remained largely unchanged since then.

MEG systems contain an array of liquid-helium-cooled low critical-temperature (low- $T_c$ ) SQUIDs that surround the head and sample the magnetic field generated by neural currents. Because this neuromagnetic field decays as a function of distance, the closer the sensors are to the head, the better the SNR and spatial resolution for MEG. The large temperature difference between the operating temperatures of low- $T_c$  technology (4 K) and the human brain (310 K) leads to a trade-off between liquid helium boil-off and SNR/resolution: the sensors housed inside standard MEG systems are typically 30+ mm from the brain, see figure 5. Furthermore, today's rigid 'one size' MEG helmets are designed to fit a large fraction of the population: their inner diameter is therefore more than 10 mm larger than the outer diameter of

the average male's head, 30+ mm larger than that of the average female, and more than 100 mm larger than that of an infant. The development of the infant MEG (Tristan Technologies, Inc.) improved the sensor-to-room-temperature standoff (to ~8 mm; the high liquid helium boil-off requires a dedicated liquefier) while targeting infants' brains, but its rigid helmet excludes subjects older than ~3 years.

High critical-temperature (high- $T_c$ ) SQUIDs cooled with liquid nitrogen to ~77 K can operate with room-temperature standoff distances of <1 mm. They could furthermore be housed inside a flexible array of cooling modules that fit snugly around arbitrary head sizes and shapes. Closer proximity to the head surface would lead to improved neuroimaging spatial resolution and SNR for adults, children, men, and women. This, in turn, can benefit MEG studies that are based on weak neural signals, such as connectivity measures, and potentially enable investigation of sources to which state-of-the-art MEG is insensitive.

#### Current and future challenges

While closer proximity to the head surface may not compensate for the higher sensor noise levels, studies with one or two high- $T_c$  SQUID sensors operating at 77 K have recently demonstrated comparable SNR [34] and source localization [38] capabilities as their low- $T_c$  counterparts operating at 4.2 K. However, in order to move the field forward, the challenge is to meet or exceed the performance of today's MEG. Simulations of sensor arrays indicate that proximity to the head surface and dense spatial sampling are more important than individual sensor SNRs: 100 or more high- $T_c$  SQUID magnetometers operating at 77 K with white noise levels of <50 fT Hz<sup>-1/2</sup> (that extend below 10 Hz) distributed evenly around the head surface with ~1 mm separating each sensor from the head surface can outperform a typical low- $T_c$

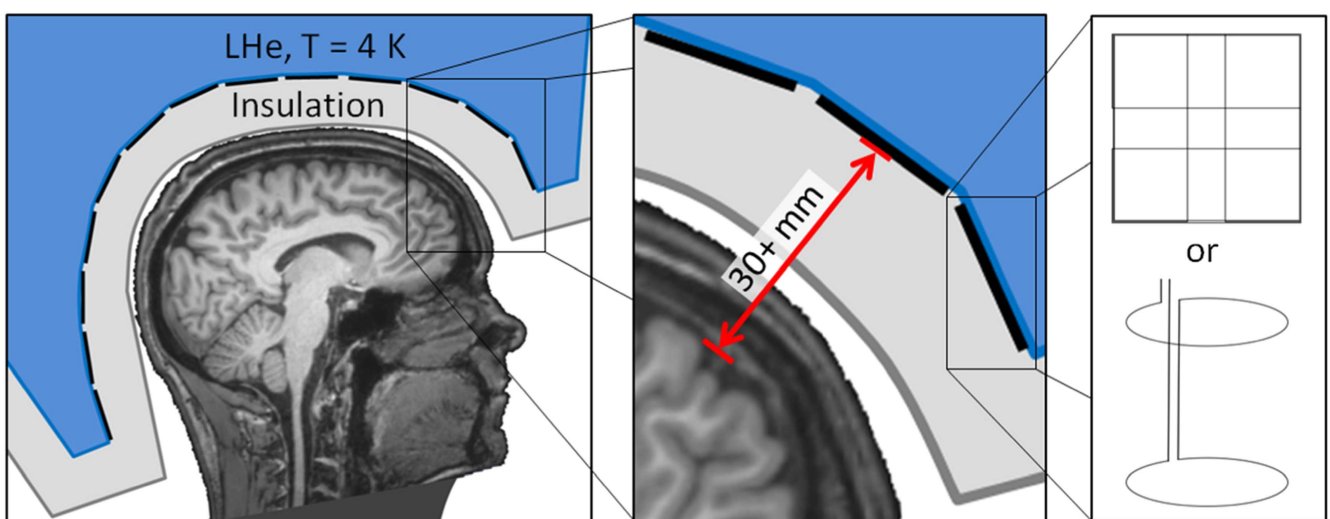


**Figure 5.** Schematic of a low- $T_c$  SQUID-based MEG system. **Left:** MRI of author JFS's head, outer dewar shell (dark grey outline), insulation space (light grey), sensor array pickup loops (black lines) and liquid helium dewar (LHe, blue). **Middle:** Inset highlighting the 30+ mm typical distance between the pickup loop of each low- $T_c$  SQUID and the subject's brain. **Right:** Standard MEG sensor pickup loop configurations: (top) a planar triple-sensor consisting of two orthogonal gradiometers and a magnetometer and (bottom) an axial gradiometer.

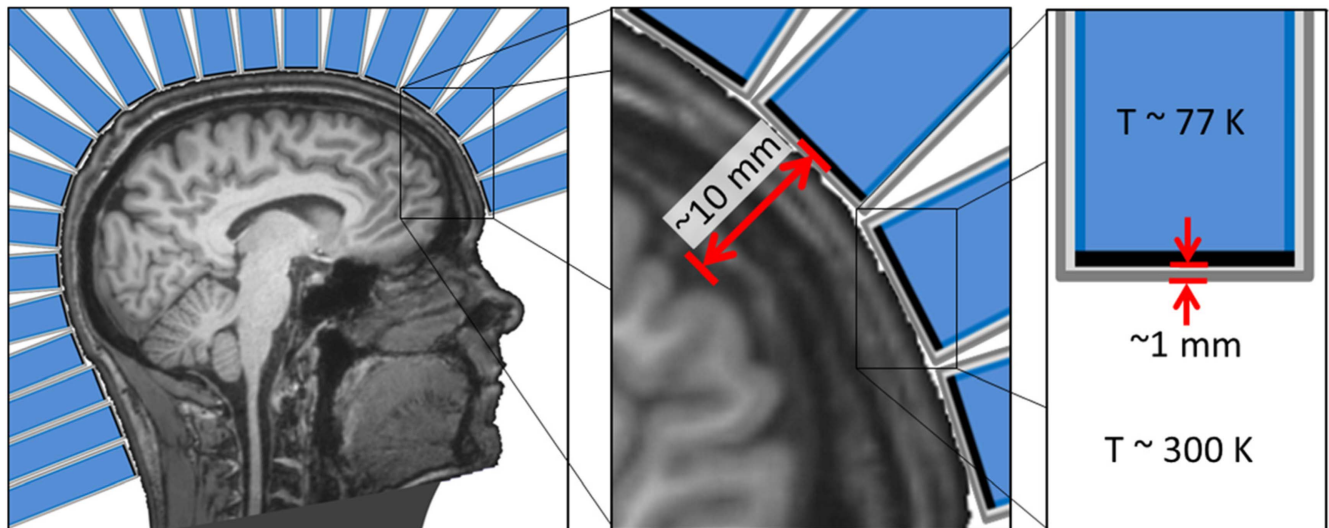


**Figure 6.** Schematic of a theoretical high- $T_c$  SQUID-based MEG system. **Left:** Head surrounded by an array of single-sensor cooling modules. **Middle:** Inset highlighting the  $\sim 10$  mm typical distance between the pickup loop of each high- $T_c$  SQUID and the subject's brain. **Right:** Detail of a single cooling module with outer vacuum enclosure (dark grey outline), insulation space (light grey), sensor (black line), and cold insert (blue).

array [39]. Today, high- $T_c$  SQUIDs have been developed with noise levels of less than  $7 \text{ fT Hz}^{-1/2}$  [40]; 77 K cryostats with warm-to-cold standoff of less than 1 mm are furthermore commercially available (e.g., ILK Dresden).

Production of a single low-noise high- $T_c$  SQUID sensor is not simple; producing hundreds is a challenge. The main candidate SQUID technologies are based on either bicrystal or step-edge junctions. The former suffers from limited availability of high-quality substrates, the latter from a technically demanding fabrication process. In both cases, significant improvements in noise levels are also challenging. Because SQUIDs are flux sensors, a typical approach to improving sensitivity in low- $T_c$  technology is to employ an inductively coupled flux transformer to increase the effective area of the sensor. However, high- $T_c$  superconducting materials are ceramic and have the lowest noise when they are made from high-quality epitaxial films whereas connections for flux transformers typically contain multiple grain boundaries that are either normal/resistive or suffer from excess  $1/f$  noise. In both cases, the low-frequency noise level limits the utility of inductively-coupled flux transformers for high- $T_c$  SQUIDs in MEG where brain signals of interest are often found below  $\sim 10$  Hz. As such, a new approach to high- $T_c$  SQUID manufacture that is scalable, reliable, and pushes the noise levels closer to that of low- $T_c$  technology is needed.

Other major challenges are more practical than fundamental. The cooling system, for example, should ideally cool hundreds of densely-packed sensors to  $\sim 77$  K in a flexible array such that each is within a few mm of arbitrary head surfaces (see figure 6) while producing less magnetic noise than that of the sensors. New approaches to co-registration, spatial filtering, and source analysis would also be needed to account for such a flexible sensor array.

### Advances in science and technology to meet challenges

Thanks to significant advances in high- $T_c$  fabrication, the goal of a more scalable and dependable process for producing hundreds of low-noise high- $T_c$  sensors is within reach. Bicrystal high- $T_c$  SQUIDs with noise levels below  $50 \text{ fT Hz}^{-1/2}$  have been repeatedly reported [34]. Step-edge junction-based high- $T_c$  SQUIDs with flux transformers reproducibly reach less than  $10 \text{ fT Hz}^{-1/2}$  with only 20% spread in the critical current [40]. Fabricating several redundant SQUIDs on the same pickup coil has the potential to improve yield by allowing selection of the best/most similar SQUIDs for a given device. With the demand for a high volume of high- $T_c$  SQUIDs driven by high- $T_c$  SQUID-based MEG, additional advancements in the technology, especially in terms of fabrication reliability, can be expected.

Further improvements in high- $T_c$  SQUID noise levels are also at hand. Fabricating multiple similar SQUIDs in series on the same pickup loop can improve field resolution. The flux noise levels of such multi-SQUID sensors have reached low- $T_c$  levels [41] and the field noise levels are predicted to reach approximately  $1 \text{ fT Hz}^{-1/2}$  with double-SQUIDs using large multilayer flux transformers [42]. Even without such redundancy, the flux noise level of a nanowire-based high- $T_c$  SQUID is on par with its low- $T_c$  counterparts [43]. While flux noise alone is not sufficient (field noise determines the ultimate performance of the sensors), these more recent developments suggest future generations of high- $T_c$  SQUID technology will be available for further advancement of high- $T_c$  SQUID-based MEG.

Cooling systems that are capable of being flexible, producing low magnetic noise, and providing warm-to-cold standoffs of  $< 5$  mm are also on the horizon. For example, micro-cryocooling technologies are reaching a promising



level of maturity. Micro-electro-mechanical system (MEMS) based Joule–Thomson type coolers [44] and microfluidic cryocoolers [45] both provide flexibility in a low-noise cooling environment. While optical refrigeration techniques are newer to the cryogenic field, their elimination of moving parts and high-pressure gas and/or liquid flows is attractive in terms of noise, but also safety. Though the technology has been used to reach steadily falling base temperatures, the recent record of 91 K [46] highlights the fact that further development (in terms of reaching base temperatures  $<80$  K) is required before optical refrigeration can be considered for high- $T_c$  SQUID-based MEG.

### Concluding remarks

High- $T_c$  SQUID-based MEG can be cheaper, safer, and better than the state-of-the-art in MEG systems. Elimination of liquid helium saves energy and money, and cryogen-free cooling systems improve user safety. The challenge is to be better at functional neuroimaging than today's MEG: theoretical improvements in SNR and spatial resolution have yet to

show their merit in the neuroscience field. Fortunately, parallel advancements in disparate fields give us reasons to be optimistic: high- $T_c$  SQUIDs are nearly as sensitive as their low- $T_c$  counterparts, micro-cryocoolers that enable on-scalp MEG with high- $T_c$  SQUIDs are available, and new approaches to experimental design and analysis are constantly being developed. With a superior system on the market, one can expect the user base for MEG to expand significantly. Such market utilization would then lead to further advancement of high- $T_c$  technology, perhaps on a scale larger than that which occurred for today's MEG and the low- $T_c$  SQUIDs on which it relies.

### Acknowledgments

This work is financed by the Knut and Alice Wallenberg Foundation (grant 2014.0102) and the Swedish Research Council (grant 621-2012-3673), the latter of which supports open access for this roadmap.

#### 4. Ultra-Low-Field-MRI

Hui Dong<sup>1,2,3</sup>, Seong-min Hwang<sup>1,4</sup>, Lixing You<sup>1,2,3</sup>, Ben Inglis<sup>5</sup>, John Clarke<sup>1</sup>

<sup>1</sup>Department of Physics, University of California, Berkeley, CA 94720, USA

<sup>2</sup>State Key Laboratory of Functional Materials for Informatics, Shanghai Institute of Microsystem and Information Technology, Chinese Academy of Sciences, Shanghai 200050, People's Republic of China

<sup>3</sup>CAS Center for Excellence in Superconducting Electronics (CENSE), Shanghai 200050, People's Republic of China

<sup>4</sup>Center for Biosignals, Korea Research Institute for Standards and Science, Daejeon 34113, Korea

<sup>5</sup>Henry H. Wheeler, Jr Brain Imaging Center, University of California, Berkeley, CA 94720, USA

##### Status

The Berkeley ULF-MRI system (figure 7) is enclosed in an aluminum shield 1.8 m on a side [47, 48]. Magnetic fields are provided by copper coils. The imaging field  $B_0$  along the  $z$ -axis is typically 132  $\mu$ T, corresponding to a nuclear magnetic resonance (NMR) frequency of 5.6 kHz for  $^1\text{H}$ . The  $x$ - and  $y$ -components of the Earth's field are cancelled. Three-dimensional (3D) images are encoded by the gradient fields  $\partial B_z/\partial z$ ,  $\partial B_z/\partial x$  and  $\partial B_z/\partial y$ . A water-cooled coil generates a pre-polarization field  $B_p$ , approximately 80 mT at the subject's head, to enhance the amplitude of the NMR signal. Subsequently, a spin-echo pulse sequence produced by the excitation coil ( $B_1$ ) manipulates the proton spins; pulse sequences used in conventional MRI, for example to measure the longitudinal relaxation time  $T_1$  and for contrast imaging, are also available. The NMR signal is detected by a second-derivative, axial gradiometer coupled to a dc SQUID in a liquid-He low-noise dewar [18]. The gradiometer loops have a diameter of 76 mm and the minimum separation of the lower loop and the subject is 25 mm. Within the signal frequency range, the system magnetic field noise, referred to the lowest gradiometer loop, is typically 0.7 fT Hz<sup>-1/2</sup> in the presence of both  $B_0$  and the frequency-encoding magnetic field gradient.

Figures 8(a) and (b) show *in vivo* 2D images of the brain with a  $2 \times 2.5 \text{ mm}^2$  pixel size obtained in about 2 min. We did not use a slice selection gradient; rather the effective slice thickness, about 80 mm, is defined by the diameter of the gradiometer loops. By using pulse sequences based on the relaxation times of various tissues and subtracting images obtained at different times in a given sequence, one can emphasize or cancel selected tissues. The images in figures 8(a) and (b) demonstrate the high level of inherent ULF contrast [48]. In earlier work [49], we obtained *in vivo* 3D images of the arm (using frequency encoding and the 1st phase encoding in-plane and the 2nd phase encoding perpendicular to the plane) with an in-plane pixel size of  $2 \times 2 \text{ mm}^2$  and a through-plane resolution of 20 mm. An example is shown in figure 8(c). The system magnetic field noise was 0.8 fT Hz<sup>-1/2</sup>,  $B_p = 40 \text{ mT}$  and

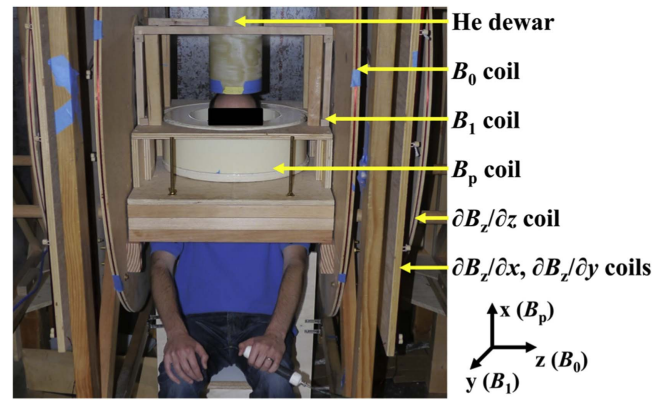
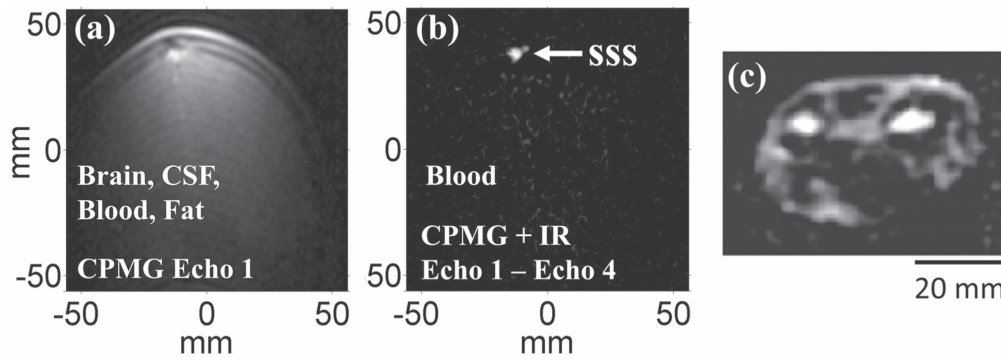


Figure 7. Berkeley ULF-MRI system.

the imaging time 5 min. Although for clinical applications it will be essential to reduce the third dimension resolution substantially, the necessary improvement appears to be achievable with existing technology. Potential applications of an upgraded system include imaging cancer without the need for a contrast agent and diagnosing traumatic brain injury (TBI) and stroke.

##### Current and future challenges

A potential advantage of ULF MRI is its intrinsic tissue contrast compared with that of clinical high-field machines, for a variety of reasons. Differences in  $T_1$  at ULF arise from the slow exchange of whole water molecules trapped in protein folds, together with intermolecular proton exchange between the free water and the OH or NH functional groups on proteins [50]. Clinical MRI machines operating at high  $B_0$  (above 1 T) can obtain images reflecting protein–water dynamics using tailored radio-frequency preparation pulse sequences before image encoding, but only within limitations. For instance, proton exchange, which is  $B_0$ -dependent via chemical shift, may overwhelm whole water molecule exchange at high field, while the heating of subjects imposes stringent restrictions on the peak amplitude and duty cycle of radio-frequency  $B_1$  pulses. ULF MRI offers negligible subject heating and chemical shift, and thus allows primary detection of slow water motions which reveal important information on protein conformation and, ultimately, on tissue status. As an example, ULF studies using rotationally immobilized protein gels (bovine serum albumin, BSA) as tissue models indicate that the frequency dispersion from 50 to 250  $\mu$ T and the divergence between  $T_1$  and the transverse relaxation time  $T_2$  may be due to interaction between free water and the local dipolar field around a protein (figure 9(a)). The sensitivity to the slow intermolecular exchange suggests that ULF MRI may be used to image stroke or TBI, where changes in protein conformation are an early indication of pathology. Degenerative conditions such as Alzheimer's disease, characterized by the abnormal build-up of proteins, are also good candidates for ULF-MRI detection. In a quite different application, a study of *ex vivo* prostate cancer from 35 patients revealed that the  $T_1$  of normal tissue was  $43 \pm 10\%$  higher (figure 9(b)) than in tumors [51]. A related potential application is the



**Figure 8.** (a) Coronal view of a brain with Carr-Purcell-Meiboom-Gill (CPMG) sequence shows brain tissue, scalp fat, cerebrospinal fluid (CSF) and blood. (b) CPMG and inversion recovery (IR), with two echoes subtracted, leave only the blood in the superior sagittal sinus (SSS). In-plane resolution is  $2 \times 2.5 \text{ mm}^2$  and slice thickness about 80 mm. (Reproduced from [48], *Proc. Natl Acad. Sci. USA* by permission). (c) 3D *in vivo* image of a human forearm, acquired with  $B_0 = 132 \text{ } \mu\text{T}$ , field gradients  $= 150 \text{ } \mu\text{T m}^{-1}$  and  $B_p = 40 \text{ mT}$ . In-plane resolution  $2 \text{ mm} \times 2 \text{ mm}$ , through-plane resolution 20 mm. Imaging time 5 min (Reproduced from [49], *Annu. Rev. Biomed. Eng.* by permission.).

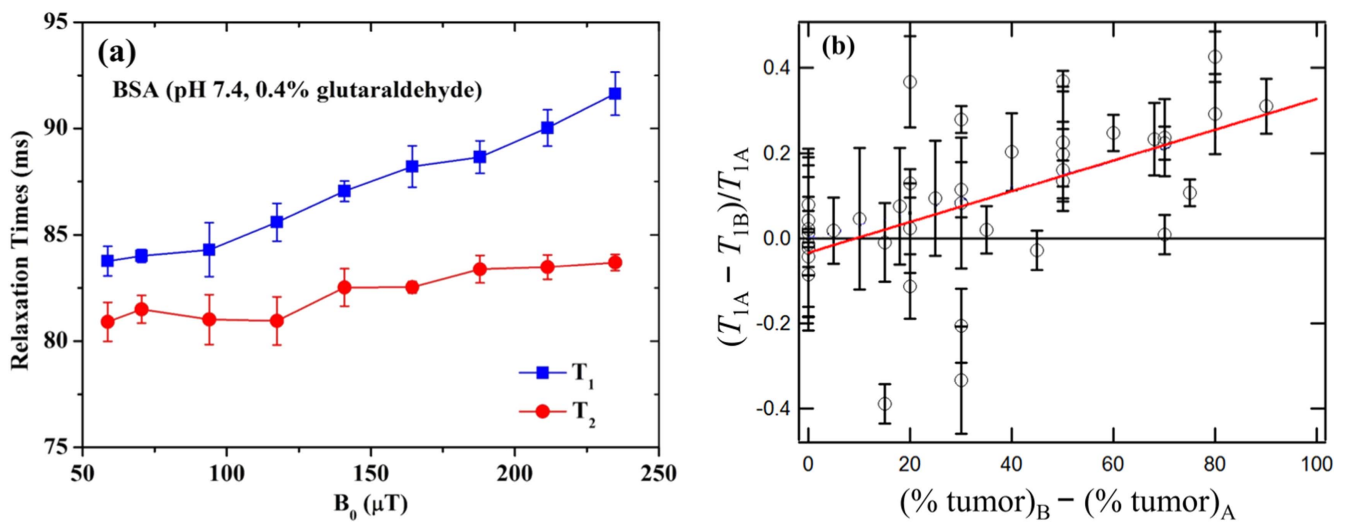


**Figure 9.** (a)  $T_1$  and  $T_2$  NMR dispersion curves of rotationally immobilized BSA gels with pH = 7.4 from 54 to 238  $\mu\text{T}$ . The proteins were cross-linked by adding 0.4% glutaraldehyde. (b) Contrast  $(T_{1A} - T_{1B})/T_{1A}$  versus  $(\% \text{ tumor})_B - (\% \text{ tumor})_A$  for two prostate tissue samples, A and B, from each of 35 patients. The red line is the least-squares fit. Percentages are from pathological evaluation. (Reproduced from [51], *MRM* by permission).

imaging of breast cancer without the gadolinium salt contrast agent required at high field. The major technical challenge now is to develop a ULF-MRI system capable of obtaining high resolution *in vivo* images in a clinically acceptable time. Furthermore, investigations of tissue model systems, which can assess the specificity of ULF MRI and thereby lead to technical developments aimed at optimizing imaging performance for different parts of the body, are very much needed.

### Advances in science and technology to meet challenges

The improvement in SNR required to meet the challenges would involve several separate upgrades of the existing system. The flux noise of our current SQUID is about  $5 \text{ } \mu\Phi_0 \text{ Hz}^{-1/2}$ . Using a SQUID with flux noise below  $1 \text{ } \mu\Phi_0 \text{ Hz}^{-1/2}$  [52], we could in principle reduce the magnetic field noise  $B_N$  from 0.7–0.8 to 0.1  $\text{fT Hz}^{-1/2}$ . To take

advantage of this very low noise, however, would require a significantly lower environmental magnetic noise than is possible with our current 1.5 mm thick Al shield. This thin shield was necessary originally because the  $B_p$  field pulse induced eddy currents in thicker shields with unacceptably long decay times. Subsequently, we developed a technique to eliminate eddy currents by applying a carefully designed pulse to a separate cancellation coil coplanar with the  $B_p$  coil. [53]. Thus, we can now use much thicker Al sheets to reduce the ambient magnetic noise substantially. A further improvement in the SNR could be achieved by redesigning the polarizing coil to have larger dimensions and to double  $B_p$  over the head to  $\sim 150 \text{ mT}$  while retaining the same turn-off time of 10 ms.

We now estimate the improvement in SNR achievable in an upgraded system compared with the value for the parameters used for the 3D arm image above, i.e. system magnetic field noise  $B_N = 0.8 \text{ fT Hz}^{-1/2}$ ,  $B_p = 40 \text{ mT}$  and imaging time 5 min. The combination of reduced  $B_N$  (a factor of 8) and

enhanced  $B_p$  (a factor of 3.75) would increase the rms SNR by a factor of 30. By increasing the imaging time to a clinically acceptable 20 min, we would gain another factor of 2 in SNR, for a total enhancement of 60. Thus, the voxel volume would be reduced to  $(2 \times 2 \times 20)/60 \text{ mm}^3 = 1.33 \text{ mm}^3$ . This resolution is comparable to that of 1.5 T clinical MRI machines.

Further improvements in the SNR could be achieved by reducing the separation between the lower loop and the subject. We note that the use of multiple sensors—already demonstrated in a MEG system combined with ULF MRI [36, 54]—would increase both the SNR and the field-of-view (FOV). Increasing the water-cooling power for the  $B_p$  coil would increase the imaging duty cycle by a factor of approximately two, and thus halve the imaging time with no reduction in SNR. While the larger FOV required for whole brain imaging would increase the imaging time for a fixed nominal resolution in any phase-encoded dimension, the availability of multiple sensors opens up the possibility of using parallel imaging acceleration schemes utilizing the spatial heterogeneity of the overall receive field [55, 56]. Multiple sensors would also enhance the SNR of signals detected from deep brain regions. We note that the diameter of our gradiometer loop is similar to the individual receive elements of phased array coils now in common use for high field MRI. We also emphasize that optimizing the detection of multiple signals for each polarizing pulse increases the temporal efficiency of prepolarization in ULF MRI.

Finally, we mention two system issues that are likely to be crucial for clinical acceptance of ULF MRI. First, although the Berkeley ULF-MRI machine requires the subject to sit in an upright position, a supine position would significantly reduce the motion of the subject and improve the image quality. Fortunately, MEG systems allowing the subject to be supine are commercially available [57], and have already been demonstrated for ULF MRI [54]. Second, an onsite refrigerator to recycle the liquid He—as for high-field MRI machines—would greatly simplify clinical use, and has

recently been introduced commercially for MEG systems [57]. The adaption of this technology for ULF-MRI would be straightforward.

### Concluding remarks

The future of ULF MRI in clinical imaging depends critically on achieving an increase in the rms SNR of at least one order of magnitude; larger increases appear to be feasible. Of the various routes to this improvement—reduced noise from sensors and ambient environment, multiple sensors, higher  $B_p$  field, and elimination of the eddy currents induced by the  $B_p$  pulse and higher duty cycle—the most challenging may be reducing the ambient noise because it will be site-dependent. The remaining issues appear to be within known limits. We believe that innovative directions for ULF MRI will likely include methods in which the attributes of  $T_1$  and  $T_2$  frequency dependence and inherent tissue contrast bring new directions not achievable with high-field MRI. These include screening for cancer without a contrast agent and detecting TBI, stroke and degenerative diseases such as Alzheimer's. As addressed elsewhere in the roadmap, other novel applications include combining ULF MRI with MEG and new techniques for neural imaging.

### Acknowledgements

We are indebted to Ian Barr for BSA sample preparation. We gratefully acknowledge support from the Donaldson Trust and the Henry H Wheeler, Jr Brain Imaging Center, University of California, Berkeley. H D thanks the National Natural Science Foundation of China (Grant No. 11204339) for support. S-m H acknowledges partial funding from the World Class Laboratory program of the Korea Research Institute of Standards and Science.



## 5. MEG–MRI: multimodal approach for spatiotemporally accurate neuroimaging

Michelle A Espy<sup>1</sup>, Risto J Ilmoniemi<sup>2</sup>, Per E Magnelind<sup>3</sup>, Andrei N Matlashov<sup>3</sup>, Jaakko O Nieminen<sup>2</sup>, Petr L Volegov<sup>3</sup>, Koos C J Zevenhoven<sup>2</sup>

<sup>1</sup>Non-Destructive Testing & Evaluation Group, Applied Engineering and Technology Division, PO Box 1663, MS-P915, Los Alamos National Laboratory, Los Alamos, NM 87545, USA

<sup>2</sup>Department of Neuroscience and Biomedical Engineering, Aalto University School of Science, PO Box 12200, FI-00076 Aalto, Finland

<sup>3</sup>Applied Modern Physics Group, Physics Division, PO Box 1663, MS-D454, Los Alamos National Laboratory, Los Alamos, NM 87545, USA

### Status

Large arrays of low-transition-temperature (low- $T_c$ ) SQUID magnetometers for MEG allow high-quality measurements of the magnetic field surrounding the head [63]. However, to take full advantage of these signals and to locate the brain activity that generates them accurately, one needs to know the conductivity structure of the head as well as the precise locations and orientations of the magnetic sensors. At present, such information comes from high-field MRI and from the manual registration of the MEG and MRI coordinate systems. Unfortunately, the registration may be off by 5 mm or more; high-field MRI suffers from susceptibility-induced distortions, and tissue conductivities are very poorly known. This makes it impossible to use MEG optimally. Also, the geometrical uncertainties (sensor positions and conductivity map) may degrade the usefulness of *a priori* information such as the constraint that primary currents are located in gray matter only.

An obvious benefit of hybrid MEG and MRI (see figure 10) is the improved workflow and convenience, if a separate MRI session is not needed. More importantly, the recording of both modalities with the same set of sensors [16, 54, 58] essentially eliminates the registration inaccuracies since, after system calibration [59], the MRI and MEG coordinate systems will be the same. This further eliminates the manual co-registration procedures. Furthermore, if we succeed in using ULF MRI [14, 49, 65] to map injected current flow [60, 64] and determine the conductivity structure accurately, we will finally have the ability to take into account the effect of volume currents accurately and use both measured data and *a priori* information in a reliable way. Moreover, MEG–MRI systems are also compatible with EEG, which can provide complementary functional information to MEG at the same high temporal resolution. However, also in EEG, knowledge of the conductivity geometry is crucial for accurate source localization.

Figures 11(a)–(b) show a comparison of MEG recorded in a hybrid MEG–MRI system at Aalto University and in a commercial MEG device at Helsinki University Central

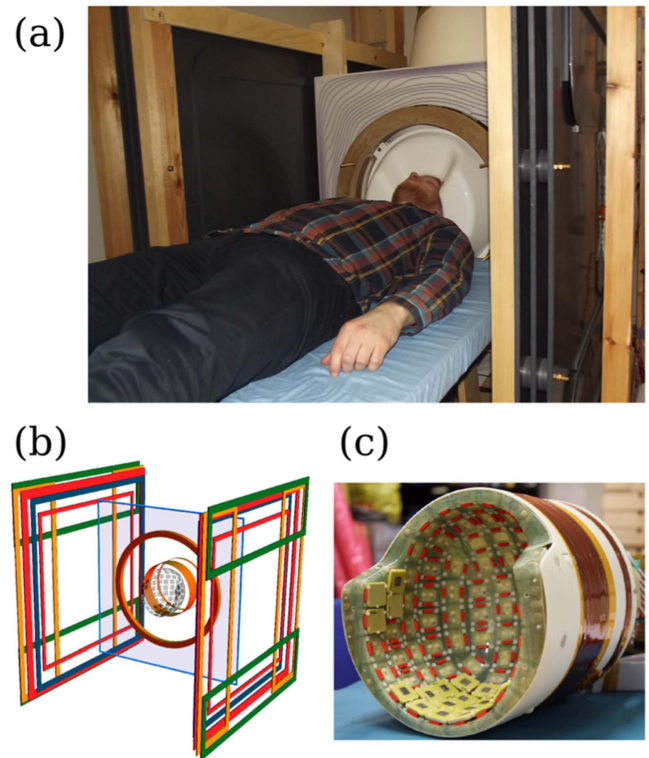


**Figure 10.** Hybrid MEG–MRI system at Aalto University: (a) photograph from inside the magnetically shielded room, (b) schematic of the coil system, and (c) photograph of the head-shaped sensor array and the superconducting polarizing coil.

Hospital, using the same stimulus protocol [36]. Reconstructed equivalent current dipoles and field patterns of visually-evoked responses at 80 ms after checkerboard stimulation onset are also displayed. Figures 11(c)–(d) show ULF MRI acquired at the Los Alamos National Laboratory at 96  $\mu$ T and a 3 T image acquired in a separate session [59]. Registered and overlaid with the ULF MRI, the equivalent dipole of an auditory response at 100 ms is presented.

While sensor types other than low- $T_c$  SQUIDs—such as high- $T_c$  SQUIDs, hybrid superconducting/giant-magnetoresistive sensors, and atomic magnetometers—have been used to record MEG and/or ULF MRI individually, no other sensor technology has, to our knowledge, been used in a hybrid multi-channel MEG–MRI system.

### Current and future challenges

Although typical MEG recordings already have a relatively high SNR, many weak brain events remain undetected or poorly located. We should aim at increasing the SNR by lowering the noise level close to the thermal limit (estimated to be about 0.1 fT Hz<sup>-1/2</sup>). However, improved knowledge of the tissue conductivity geometry is needed to take full advantage of the additional detail in the MEG recordings. For accurate spatial information, we should thus improve the spatial resolution and SNR as well as the speed of data acquisition of ULF MRI.

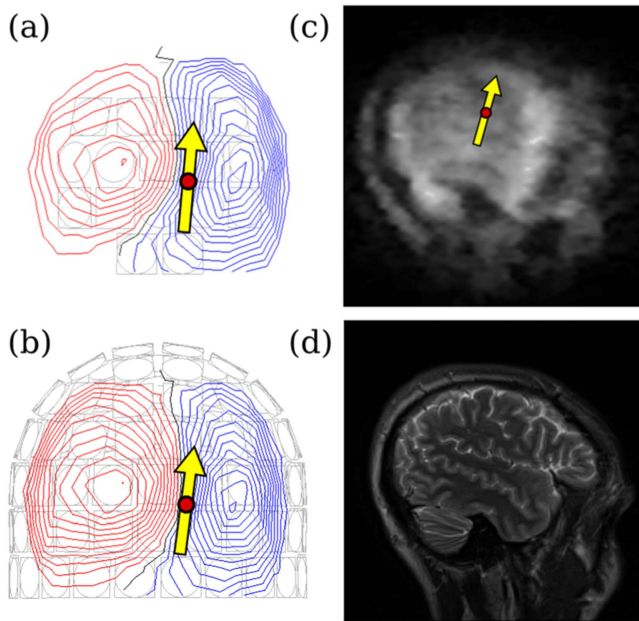


**Figure 11.** Equivalent dipoles and field patterns of the visually-evoked responses—presented using a spherical-harmonic expansion of data—using (a) the MEG–MRI system and (b) state-of-the-art MEG with the same stimulus protocol. MRI slices (c) at  $96\ \mu\text{T}$ , with the registered equivalent dipole of the auditory response overlaid, and (d) from an uncoregistered 3 T image acquired separately from the same subject.

While ULF-MRI sequences for measuring electric current density provide, in principle, more complete information of the three-dimensional field than their high-field-MRI counterparts, the optimal way of collecting information of injected current flow and turning it into conductivity information remains unknown. The sequences rely on rapid cycling of the main magnetic field  $B_0$  [61], as well as on accurate ULF-MRI phase images, which in turn require fast high-precision spin flipping, which is not addressed by traditional MRI methods.

Accurate knowledge of the conductivity geometry enables the use of detailed *a priori* information about the source current distribution for locating neuronal activity in the brain. To achieve this, methods must be developed that allow one to utilize different types of *a priori* information that are related to the geometrical and conductivity information provided by ULF MRI.

ULF MRI has yet to demonstrate functional imaging, i.e., imaging of neuronal activity, for instance, through the indirect changes in blood flow/volume or the direct effect of local neuronal currents on the spins in tissue. The combination of functional tomographic imaging with MEG in the same system would provide spatial constraints for the inverse problem

solution and reduce the solution space dramatically. A truly multi-modal imaging system would then be realized.

### Advances in science and technology to meet challenges

The optimum sensor array and imaging sequence for information collection are still open questions in MEG–MRI. One obvious way to improve the SNR, however, is to lower the noise floor. While lowering the sensor noise is key to the development of both MEG and MRI, it comes with additional challenges for the rest of the system. The additional sensitivity is lost when thermal magnetic noise from the polarizing coil or the liquid-helium dewar becomes dominant. Similarly, the electronics driving current pulses into the ULF-MRI coils produces magnetic field noise that is detectable especially by magnetometers that measure along the applied field. The amplifier electronics thus require an even larger dynamic range than required for the SQUID sensor readout [61].

Another issue concerns transient effects, caused mainly by the pulsed polarizing field that enables the measurement at ultra-low frequencies but, in addition, induces eddy currents in the walls of the magnetically shielded room. The eddy currents decay slowly, not only saturating the SQUID readout, but also seriously distorting the nuclear spin dynamics in the tissues to be imaged. For the polarizing pulse, the eddy-current issue was successfully mitigated using a self-shielded coil design [36]. However, improved image quality may require a larger polarizing coil and pulse amplitude, which severely increase the induced currents. These remaining eddy-current transients may be dealt with by designing a DynaCan setup [53]. A superconducting polarizing coil can also be left magnetized by the pulses, which requires further development of in-sequence demagnetization of the coil. Also the SQUID sensors are exposed to the pulsed fields, and their recovery after a pulse is associated with an amount of transient noise that depends on the type of superconducting pickup coil [24, 22, 62]. The recovery period should be made short compared to tissue relaxation times.

### Concluding remarks

The combination of MEG and MRI in a hybrid system has been demonstrated in limited scale thus far. Technological development of ULF MRI in particular is needed to increase the quality of the images and to enable this promising method to be fully exploited. The MEG recorded in hybrid systems has been shown to be on par with recordings in state-of-the-art commercial MEG systems. The unique possibilities of ULF MRI in current-density imaging can provide valuable conductivity information for improving the accuracy of MEG source localization in hybrid multi-channel MEG–MRI.



## 6. Neuronal current imaging in the brain via ultra-low-field MRI

Nora Höfner, Martin Burghoff, Rainer Körber

Physikalisch-Technische Bundesanstalt (PTB), Abbestraße 2-12, 10587 Berlin, Germany

### Status

Decoding complex cognitive processes from the macroscopic down to the cellular level is a highly topical issue in neuroscience. It is essential to understand the information processing of the human brain entirely and to gain more insight that might possibly support new treatment methods of neurological disorders such as Alzheimer's disease or epilepsy. Its realization necessitates a measuring device that tracks neuronal impulses simultaneously with a high temporal and spatial resolution. However, currently available non-invasive techniques do not cover both needs. On the one hand, direct measurement methods like EEG and MEG detect electric and magnetic field distributions of neuronal activities over the head surface with a temporal resolution below one millisecond [66]. The low localization accuracy—in the centimetre range [66]—results from the ill-posed inverse problem when performing source reconstruction on the basis of simplified assumptions regarding tissue conductivities, geometries or number of sources [25]. On the other hand, detection methods like fMRI or functional near-infrared spectroscopy have a spatial resolution in the millimetre and centimetre range respectively and a temporal resolution of about 1 s. However, fMRI does not provide a direct image of the brain's activity, because it is based on the blood-oxygenation-level-dependent (BOLD) contrast caused by susceptibility changes near activated brain areas due to a varying level of oxygenated haemoglobin [67]. The combination of the millimetre resolution of MRI and the detection of the influence of neuronal magnetic fields on the nuclear spin precession forms the basis of NCI. However, when NCI is attempted in the tesla range, susceptibility artefacts of the BOLD-effect seem to mask the small influence of neuronal magnetic fields [68]. As BOLD scales with the applied magnetic field, reducing the field down to some microtesla appears to be a promising approach. In this case, susceptibility artefacts will decrease to a negligible magnitude while the amplitude of the neuronal fields is unaffected and dominates [69]. This chapter discusses NCI via ULF MRI and expected neuronal-current-dependent contrast mechanisms [69, 70]. Two measurement principles are suggested. The resonant mechanism aims to identify discrete frequency components of neuronal magnetic fields (up to 2 kHz) by their action as a resonant tipping pulse, provided that they match the Larmor condition of the read-out field [69, 71]. The DC-mechanism detects neuronal magnetic fields by their superimposition with the read-out field thus causing local frequency changes and/or increased dephasing.

### Current and future challenges

The read-out field reduction for ULF MRI by 5–6 orders of magnitude to the microtesla regime leads to an enormous loss in signal strength, which can be compensated to some degree by applying prepolarizing fields and using very sensitive SQUID sensors [49]. For the resonant mechanism, switching from prepolarizing to read-out field should be done adiabatically leaving the magnetisation aligned along the read-out field so that it can be subsequently tilted by resonant neuronal fields [69]. The induced precession can be localised by applying spatial encoding gradients [69, 71]. In addition, this method could provide the possibility of identifying correlated sources [71]. Phantom studies were performed under simplified conditions, as a proof-of-principle of the method, but showed an enormous lack of SNR as well which may be difficult to overcome [69, 71, 72].

For the DC-mechanism, a precession needs to be induced first by a  $\pi/2$ -pulse or non-adiabatic switching between the perpendicularly aligned prepolarizing and read-out fields [72]. Spatial encoding gradients would indicate the location of the activity. Currently, this method is suitable for evoked long-lasting activities and could reach a temporal resolution of about 50–100 ms. Phantom measurements, pictured in figure 12, demonstrate the DC-mechanism under near-physiological conditions and show that the SNR needs to be increased by at least a factor of 2 to have a chance of realizing NCI via ULF MRI. As conductivity and source models of these experimental phantom data were simplified, they can serve only as a guide concerning the required SNR enhancement necessary for *in-vivo* NCI. Of course, only *in-vivo* measurements can confirm predicted contrast mechanisms with respect to primary and secondary currents within and around real active neuronal structures [70].

These *in-vitro* results demonstrating the two proposed measurement principles indicate the biggest challenge for realizing NCI via ULF MRI: obtaining a sufficient SNR in order to resolve the faint influence of neuronal magnetic fields on the spin precession.

### Advances in science and technology to meet challenges

The development of an ULF-MRI setup for NCI with sufficient SNR represents an optimization problem with versatile levers. This can be obtained (i) by accomplishing a low noise level and/or (ii) by increasing the prepolarizing field to boost the magnetization. However, the application of high currents to a resistive prepolarizing coil demands cooling or a reduced duty cycle to avoid overheating, especially as imaging sequences and averaging for SNR enhancement require numerous repetitions [73]. If the prepolarizing coil is made of a type-II superconductor, the prepolarizing field should not exceed its lower critical field  $H_{c1}$ , to avoid the penetration of flux into the material that may generate remanent perturbing magnetic fields [36]. Trapped flux is also critical in pick-up coils made of type-II superconductor leading to field

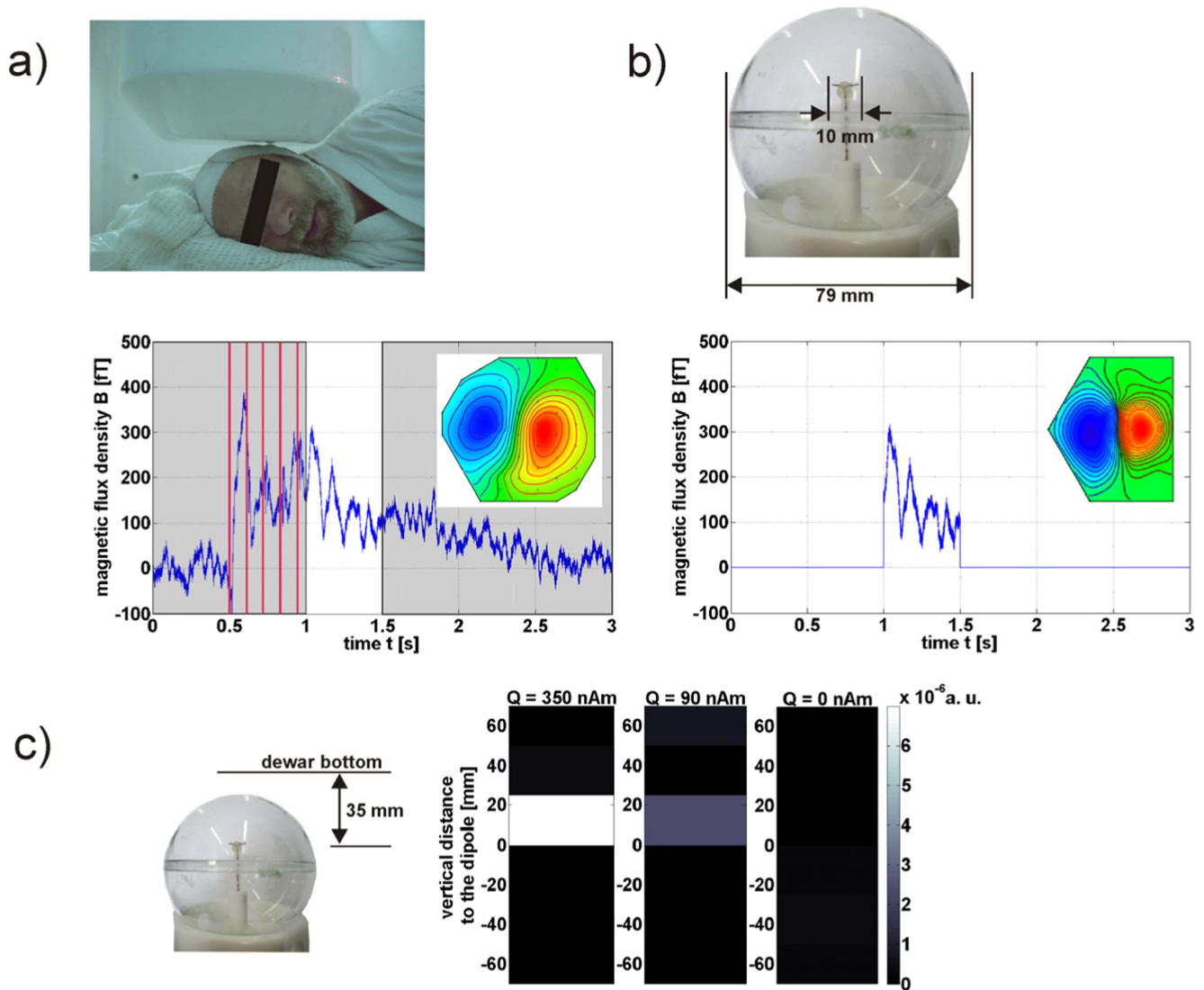


**Figure 12.** (a) Median nerve stimulation evokes low-frequency brain activity. After the stimulation, a maximum equivalent current dipole (ECD) strength of 50 nAm with a depth of 35 mm was estimated from the magnetic field distribution of MEG measurements [72]. (b) This neuronal magnetic field distribution is simulated using a current dipole and applying a driving current according to the detected time curve over 0.5 s after the stimulation. The current dipole (length  $\sim 10$  mm) is located in a head phantom with a realistic distance to the dewar bottom (35 mm) and operated within a copper-sulfate solution, imitating the relaxation of grey brain tissue ( $T_1 = 100$  ms,  $T_2^* = 100$  ms). (c) For the NCI experiment the prepolarizing field of 30 mT was followed by phase-encoding gradients to define horizontal slices (slice thickness of 25 mm). 14 averages were acquired with a total measurement time of 45 min. The dipole is located in the centre between neighbouring slices to break its field symmetry avoiding signal cancellation [72]. In order to image the very small dipole influence, the magnitude masked phase difference of two differentially affected measurements (dipole applied and not applied) is plotted. Weak residual signals appear in the slice with the smallest distance to the sensor system thus detected with the highest sensitivity. The residual signals scale with the applied ECD-strength  $Q$  and the absence of a residual signal for no dipole operation demonstrates the stability of the setup. The minimal detectable ECD-strength amounts to  $Q \sim 90$  nAm (peak value) for a system noise level of  $1 \text{ fT Hz}^{-1/2}$  at 415 Hz.

distortions [24] and excess low-frequency noise [21]. Of course, all other materials in the immediate vicinity of the sample should be selected carefully with respect to their magnetic remanence. Degaussing after prepolarization could remedy this situation with the trade-off of an increased dead-time and a corresponding signal loss [24]. In general, the number of components close to the sensor generating thermal noise—usually metals—should be kept at a minimum. The noise of the prepolarizing coil, inevitably located close to the sample and hence to the sensor, is critical and can be reduced by using litz wire. In addition, current noise from sources

driving idle gradient coils and the prepolarizing coil can be avoided by disconnecting them during data acquisition. Sensor sensitivity can be enhanced by using comparably large pick-up coils. When the system noise is reduced such that thermal noise from the tissue below  $0.1 \text{ fT Hz}^{-1/2}$  (when resting state activity is negligible, cf chapter 1) dominates, averaging appears to be the only remedy for noise reduction.

The application of magnetic field pulses, in particular prepolarizing pulses, induces eddy currents in the walls of the magnetically shielded room. The distorting effects of the resulting magnetic-field transients on the spin dynamics need

to be met not only for ULF MRI but also for NCI. Self shielded coils or a dynamic cancellation technique minimise these effects [36, 53]. Regarding the DC-mechanism it is essential that the reproducibility of transients or dynamic cancellation pulses between repetitions is sufficient to avoid false-positive results when determining the influence of neuronal fields via difference signals (see figure 12(c)).

### Concluding remarks

Currently the detection limit for NCI is close to the estimated equivalent current dipole for long-lasting neuronal fields. As both the noise level and the prepolarizing field strength can still be improved, possibly increasing the SNR by one order of magnitude, the realisation of NCI via ULF MRI seems within reach. In this case, a spatial resolution in the millimetre range and a measurement time of several minutes can

potentially be achieved. Furthermore, implementing the resonant mechanism seems difficult [72]. However, realising NCI only for long-lasting neuronal activities with a limited resolution would still be of enormous importance and could serve as a reference for the localization accuracy of MEG and EEG. In addition, on the basis of NCI research and development, injected currents could also be imaged to determine the individual conductivity distribution of the head. This information can be used to stabilize the solution of the inverse problem for MEG and EEG (cf chapter 5).

### Acknowledgement

This project has received funding from the European Union's Horizon 2020 research and innovation programme under grant agreement No 686865.

## 7. Magnetic nanoparticles for immunoassay

Keiji Enpuku<sup>1</sup>, S Y Yang<sup>2</sup>, and Jen-Jei Chieh<sup>3</sup>

<sup>1</sup>Kyushu University, Fukuoka, Fukuoka Prefecture, Japan

<sup>2</sup>MagQu Co. Ltd., No.12, Ln. 538, Zhongzheng Rd, Xindian Dist., New Taipei City 231, 23141 Taiwan

<sup>3</sup>National Taiwan Normal University, No. 88, Section 4, Ting-Chou Rd, Taipei 116, Taiwan

### Status

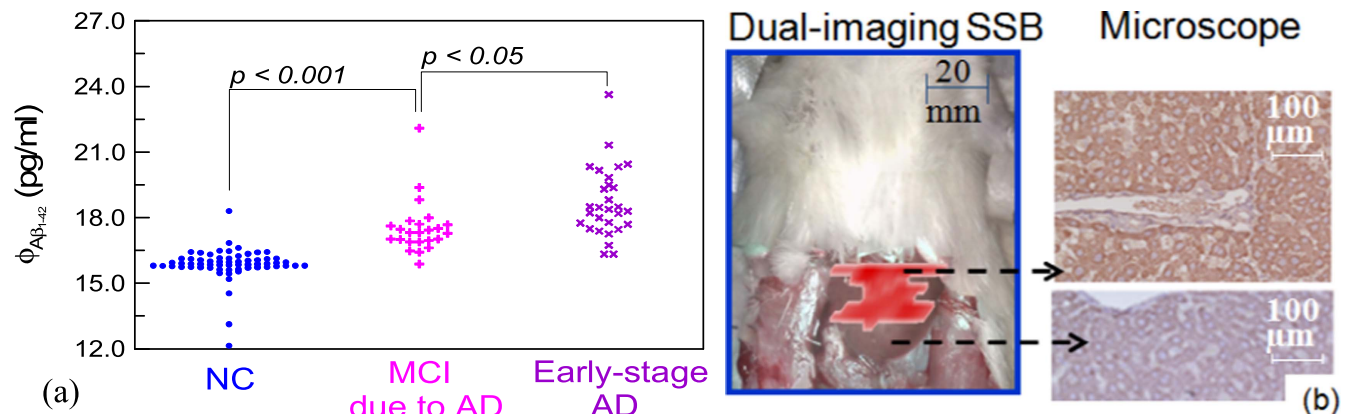
Bio-functionalized magnetic nanoparticles (or magnetic markers) have been widely used in biomedical applications [74]. Recently, magnetic immunoassay techniques that utilize magnetic markers and SQUIDs have been developed for medical diagnosis. One of the merits of these magnetic methods is that the liquid-phase detection of biological targets can be performed by using the Brownian relaxation of the markers. Hence, unlike in conventional optical methods, the time-consuming washing process for marker separation can be omitted. In liquid-phase detection, bound markers that couple to the targets have been magnetically differentiated from the unbound (free) markers by using the difference in their magnetic properties, such as ac susceptibility [75–77], magnetic relaxation [78, 79], and remanence [80, 81]. The weak (picotesla-range) signals from the bound markers can be precisely measured with a SQUID sensor. To date, the highly sensitive detection of various biological targets has been demonstrated, confirming the usefulness of magnetic immunoassay techniques. These techniques have also been expanded to enable the detection of markers in humans (and animals) for *in-vivo* diagnosis.

In figure 13, examples obtained using magnetic methods are shown. Figure 13(a) presents the dot plot for the concentrations  $\phi_{A\beta_{1-42}}$  of amyloid beta ( $A\beta_{1-42}$ ) proteins detected in human blood (plasma) samples by using an ac susceptibility method called immunomagnetic reduction (IMR) [75].  $A\beta_{1-42}$  is a well-known protein related to the occurrence of Alzheimer's disease. Most of  $A\beta_{1-42}$  protein molecules exist in cerebrospinal fluid. It is very rare for a portion of  $A\beta_{1-42}$  to be released to peripheral blood. Thus, the concentration of

$A\beta_{1-42}$  is expected to be ultra-low, which hopefully could be detected by an ultra-sensitive method. The subjects included normal controls (NC), patients with mild cognitive impairment (MCI), and patients with early-stage Alzheimer's disease (AD), which are grouped according to neuropsychological tests and clinical symptoms. All subjects in figure 13(a) are older than 50 years and were recruited at the National Taiwan University Hospital.

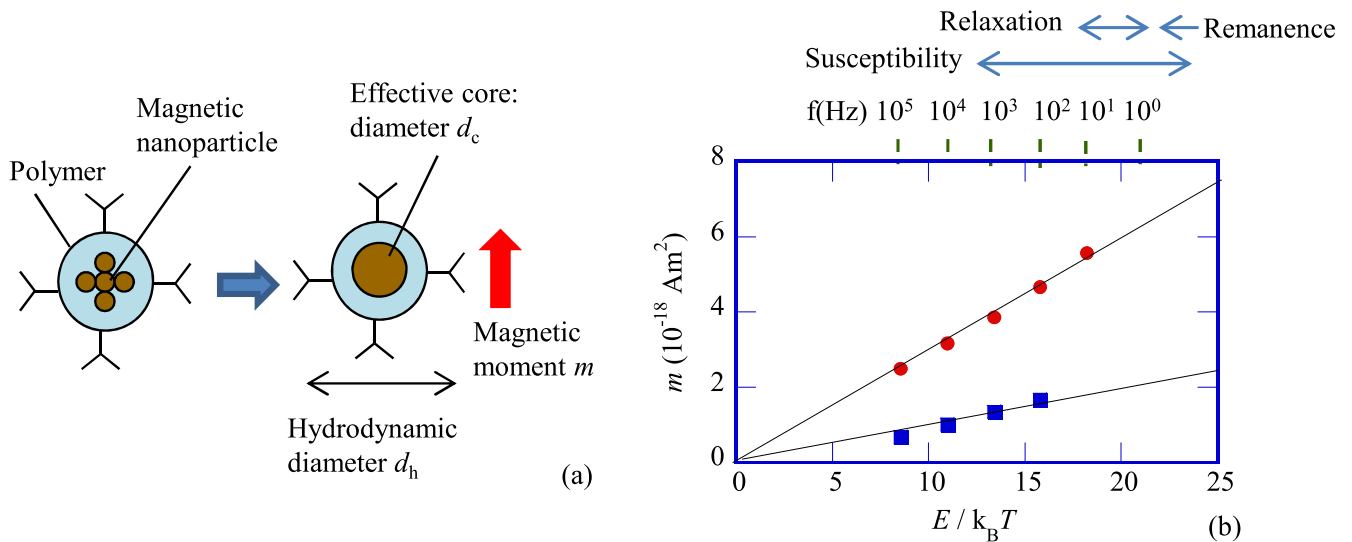
In figure 13(a), the vertical axis represents the concentrations of  $\phi_{A\beta_{1-42}}$ , while the horizontal axis is used for grouping subjects into different categories. The experimental result from one subject is represented by one dot. In order to show the number of subjects with the same concentration of  $A\beta_{1-42}$ , the dots with the same  $\phi_{A\beta_{1-42}}$  were lined up in the horizontal axis. From the spread of the dot plot, therefore, we can see the statistics of the experimental results in each category. As shown in figure 13(a), a clear difference in  $\phi_{A\beta_{1-42}}$  between normal controls and patients is evident, i.e. the  $p$  value is smaller than 0.05 via a T-test analysis. Therefore, MCI and AD patients can be diagnosed by assaying plasma  $A\beta_{1-42}$ . It is worth noting that  $\phi_{A\beta_{1-42}}$  is below  $50 \text{ pg ml}^{-1}$ , which is quite low. Thus, these results demonstrate that SQUID-based IMR can be used to assay these low concentrations of biomarkers in blood for early-stage diagnosis or screening.

Figure 13(b) shows detection of inner liver tumors measured using an ac susceptibility method called dual-imaging scanning SQUID biosusceptometry (SSB) [76, 77]. In the experiment, magnetic markers conjugated with alpha fetoprotein (AFP) antibodies were injected into a rat, which were specifically bound to the AFP antigens on the surfaces of liver tumors. Then, the ac signal field from the tumor-targeted markers was sensitively detected with the SSB. In the left part of figure 13(b), the result is shown by a red-spot magnetic image, simultaneously co-registering with a photograph of the torso surface of the rat. The feasibility of tumor discrimination was verified with tissue stain, the gold standard of clinical discrimination. As shown in the right part of figure 13(b), a good consistency is obtained between the red region in a magnetic image of an abdomen and the darker expression in the microscope image of stained liver tissues. It



**Figure 13.** Examples of magnetic immunoassay techniques. (a) Detection of  $A\beta_{1-42}$  in human plasma samples. (b) Images of rat liver tumors. Both results were obtained with high- $T_c$  SQUIDs.





**Figure 14.** (a) Schematic of a magnetic marker, where the marker consists of aggregated nanoparticles and the agglomerate is approximated by an effective magnetic core with diameter  $d_c$ . (b) Relationship between  $m$  and  $E$ . Results obtained for two markers are shown.

has been shown that tumor discrimination using SSB is more powerful than tissue stain [77].

### Current and future challenges

Although the detection of various targets has been performed and the merits of SQUID-based detection methods have been demonstrated, there are many challenges that must be addressed to further improve the reliability, stability, and sensitivity of magnetic methods. First, markers with well-controlled magnetic properties and good dispersion (or no aggregation) in solution are necessary. Unfortunately, such markers have not yet been fully established because of their complicated properties. Therefore, it is essential to develop markers that are suitable for use in magnetic immunoassay techniques to further improve these methods.

It must be noted that the three detection methods, i.e., ac susceptibility, magnetic relaxation, and remanence measurement, require markers with different magnetic properties. Therefore, the SQUID system and detection method should be optimized based on quantitative characterization of the markers. The SQUID system should also be sufficiently robust against interference from the excitation field. The excitation field used to magnetize markers can be up to a few millitesla, and the system must maintain stable operation even in this situation.

In the liquid-phase immunoassay method, the Brownian relaxation of the markers is a key property in determining the detection sensitivity, in addition to the SQUID system noise. In this method, the magnetic signal from the markers that are bound to the target is differentiated from that of the unbound (free) markers by using Brownian relaxation. If the Brownian relaxation deteriorates, a so-called blank signal is generated by the free markers, and it degrades the sensitivity of the liquid-phase immunoassay [81]. Therefore, it is important to clarify the factors that cause Brownian relaxation to deteriorate and to develop a means of avoiding this problem. In

*in-vivo* applications, the spatial resolution of the marker position measurements in the human body is an important issue, as is the detection sensitivity [79]. Since marker detection is performed by using a contour map of the markers' signal field, it is important to obtain a high-quality contour map in a short measurement time. Multichannel sensor systems are quite effective in this regard. It is also necessary to develop an imaging technique to reconstruct marker distributions from contour maps precisely.

### Advances in science and technology to meet challenges

The markers used in the aforementioned techniques are usually composed of aggregated magnetic nanoparticles, as schematically shown in figure 14(a). When the markers are used in an immunoassay, their key parameters are their magnetic moments  $m$  and relaxation times. A high  $m$  value is desired to obtain strong marker signals. On the other hand, the required relaxation time depends on the particular detection method. The relaxation time of the free markers in a suspension is given by the Brownian relaxation time  $\tau_B$ , whose value ranges from  $10 \mu\text{s}$  to  $1.3 \text{ ms}$  for hydrodynamic diameters  $d_h$  of  $30\text{--}150 \text{ nm}$ . The relaxation time of the bound (immobilized) markers is dominated by the Néel relaxation time  $\tau_N$ , which is determined by the anisotropy energy  $E$  according to  $\tau_N = \tau_0 \exp(E/k_B T)$ . In order to perform liquid-phase detection, the relaxation times must satisfy the condition  $1/\tau_N < f < 1/\tau_B$ , where  $f$  is the measurement frequency.

In figure 14(b), the relationship between  $m$  and  $E/k_B T$  is shown for two different commercial markers [82]. The upper horizontal axis represents the frequency corresponding to the Néel relaxation time, i.e.,  $f = 1/(2\pi\tau_N)$ . The typical frequency ranges used in each detection method are also shown by arrows. Figure 14(b) reveals the following basic characteristics of the markers. (1) The  $m$  and  $E$  values are distributed within the markers. Therefore, only the portions of markers with the

proper  $m$  and  $E$  values contribute to the magnetic signal. (2) An appropriate value of  $E$  is required for each detection method. Thus, it is necessary to select markers that have large portions with  $E$  values in the required range. (3)  $m$  is proportional to  $E$ . Since the  $m$  value gives the signal from a single marker, this value determines the sensitivity of the detection system.

We note that the  $E$ - $m$  curve of the markers is different from that of the bulk material and that the  $E$ - $m$  curves for different markers also vary; the physics behind these differences has not yet been fully explained. Based on  $E$ - $m$  curves, markers suitable for use in magnetic immunoassay techniques can be selected or developed. Then, the detection system design can be optimized.

### Concluding remarks

The SQUID system and detection methods for *in-vitro* and *in-vivo* medical diagnosis have already been developed, and the highly sensitive detection of various targets has been demonstrated. In order to use magnetic methods clinically, however, users must be convinced of the advantages of this method compared to the conventional method. It is also necessary to develop magnetic markers suitable for these applications to further improve magnetic techniques. Therefore, the complicated properties of magnetic markers should be quantitatively characterized and SQUID systems and detection methods should be optimized based on the markers' properties.



## 8. The commercial roadmap

Jukka Knuutila, Petteri Laine, Jukka Nenonen

Elekta Oy, PO Box 34, FI-00531 Helsinki, Finland

### Status

It has been estimated that during the first two decades of SQUIDs (ca 1972–1992), slightly more than 1000 SQUID sensors were employed in all biomagnetic applications [83]. After the introduction of the first MEG systems covering the whole cortex around 1992 (e.g., [83, 84]), about 250 commercial MEG systems (including replacements and upgrades) with over 50 000 SQUID sensors have been installed worldwide by the end of 2015 (figure 15).

Various attempts have been made to commercialize multichannel SQUID arrays for biomagnetic applications such as MEG or adult and fetal MCG (see, e.g., [83]). However, only MEG has proven commercially viable with the annual production of 5–15 commercial whole-head systems. In early 2016, the main commercial providers were Elekta (elekta.com), MEG International Services Ltd (ctfmeg.com), and Tristan Technologies (tristantech.com). In addition, three companies announced their plans to enter the MEG market. These companies were Compumedics Ltd (compumedics.com), Ricoh Co., Ltd (ricoh.com), and York Instruments Ltd (york-instruments.co.uk). Figure 16 displays three examples of commercial MEG systems.

MEG systems have been employed both in basic brain research and for clinical patient studies (chapter 2). Today, commercial expectations are focused on clinical applications such as epilepsy and pre-surgical functional mapping. Annually, about 10 MEG systems are delivered for these applications. Active clinical research is ongoing in MEG studies aiming to find novel biomarkers in various neurological and psychiatric diseases, as well as in drug studies. Emerging new clinical indications (e.g. stroke, head trauma and degenerative disorders [63]) are anticipated to bring a substantial increase in the number of new MEG systems. According to some industry estimates, the market could grow to tens of units per year fueled by such scientific advances enabling more routine clinical application of the technology.

### Current and future challenges

Although there has been significant investment and effort, the volume of the market for commercial MEG systems has remained limited. The small market volume, combined with the heavy regulations in the medical device business and the continuing need for development, sets challenges to the companies operating in the field.

To date, the only technically practical and sufficiently sensitive sensor for MEG has been the low- $T_c$  SQUID, although other potentially promising sensor types have also been introduced, such as optically pumped magnetometers [85], GMR-based ‘mixed sensors’ [86], and high- $T_c$  SQUIDS (chapter 3).

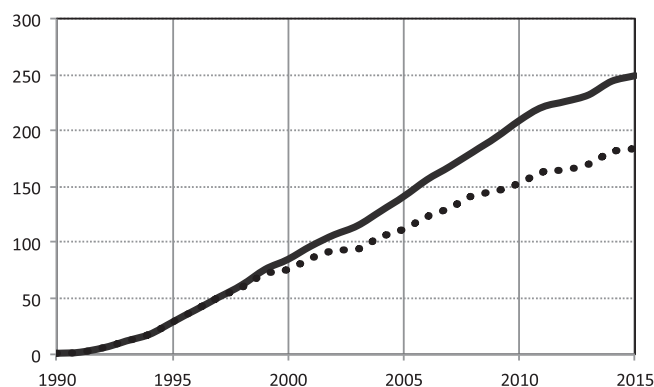


**Figure 15.** Cumulative number of installed commercial multichannel SQUID systems, including replacements and upgrades (solid line) and cumulative number of systems in use as of 2015 (dotted line).

Regardless of the sensor type, the estimation of the neural sources underlying the MEG signals is limited by the sensor noise and the magnetic interference from sources external to the brain. Hospitals are electromagnetically hostile environments for ultrasensitive magnetic field measurements, requiring heavy magnetic shielding. Large two- or three-layer magnetically shielded rooms (MSR) are effective but expensive, and require a large space. In addition, the low- $T_c$  SQUID sensors require liquid helium to operate. A typical MEG system needs to be refilled once or twice per week. The cost and space needed for the magnetically shielded room and the lack or limited availability of liquid helium for regular fillings have been among the biggest obstacles for acquiring and maintaining MEG systems.

The main goal in MEG studies is to infer information about neural processes based on the weak magnetic field produced by the associated neural currents. The weakness of the signals can be overcome by increasing the sensitivity of the sensors; however, susceptibility to ambient interference fields also increases. Another challenge specific to MEG is the possible movement of the subject's head during recording in respect to the stationary physical sensor array. Patients may also have therapeutic stimulators that are magnetic or there may be magnetic residue from previous surgery in their body.

Due to the technical complexity of MEG systems and the data analysis methods, the user experience of MEG recordings and analysis has not yet reached a level expected by busy clinical users. Therefore, the whole workflow from patient preparation through recordings and data analysis to a clinical report is still challenging and time-consuming even for clinical experts. MEG also has to compete with other imaging methods (e.g., functional MRI, SPECT, PET and high-density EEG). Increasing the commercial viability of MEG in current clinical applications requires better MEG-specific clinical analysis software with more sophisticated and automated clinical workflows in order to increase the patient throughput. In the future, development of new clinical indications is vital for widening the clinical MEG patient population and customer base.

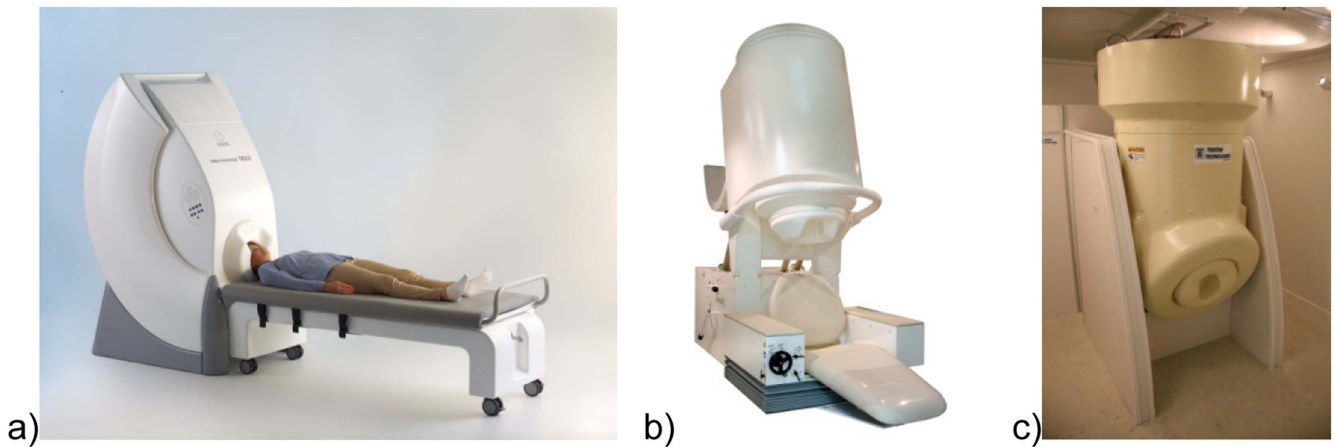


**Figure 16.** Examples of commercial whole-head MEG systems: (a) Elekta Neuromag® TRIUX, (b) CTF cMEG, photo used with permission of CIF MEG International Services LP. (c) Tristan MAGView™ Biomagnetometer, photo used with permission of Tristan Technologies Inc.

### Advances in science and technology to meet challenges

The cost of liquid helium can be reduced or eliminated with helium recycling systems utilizing cryocoolers. In an open-loop recycling system, the gas boiling from the MEG system is liquefied into a storage dewar which is then employed in manual refills. Typically some helium is lost during the refills, which has to be compensated with regular gaseous or liquid helium deliveries.

A more advanced system is displayed in figure 17, which shows a closed-loop zero helium boil-off recycler (Elekta Oy) integrated in a commercial MEG system. During MEG data acquisition, the cryocooler cold head and compressor are offline. The gas storage system collects and pressurizes the helium gas evaporating from the liquid helium dewar of the MEG probe unit through the helium gas line. During helium liquefaction, the cryocooler cold head and compressor are online. The gas storage system releases helium gas that flows through the helium gas line towards the liquid helium dewar of the MEG probe unit. The cryocooler cold head liquefies helium gas within the dewar vessel. The operation of the internal helium recycler is controlled by the control system inside the helium recycler cabinet. This kind of system makes the user independent of the helium deliveries and reduces the running cost.

The development of light-weight MSR and active shielding technologies such as internal active shielding provides excellent magnetic shielding with significantly smaller size, weight, and cost [87]. Recent sensor development made in conjunction with MEG-MRI systems promises new generation low- $T_c$  SQUID sensors with increased sensitivity and better tolerance of ambient magnetic fields [88] (see also chapter 1). This kind of sensor could also be utilized in clinical MEG systems that are operated in a magnetically hostile environment with reduced magnetic shielding, or even unshielded.

MEG measurement technology has taken huge steps forward since the early days when the number of recording channels was one or only a few. Novel interference and noise

suppression methods have been developed for modern MEG systems with more than 150 recording channels, such as the signal space projection, SSP [20] and signal space separation, SSS [89]. Head movement correction together with the temporal extension of signal space separation, tSSS, has proven to be invaluable in several MEG patient studies involving artifacts induced by magnetized pieces on the scalp, dental work, implanted stimulators, and head movements [90].

Several research centers and groups are continuously developing MEG data analysis methods, such as tools for neural current source imaging and brain activity network analysis. Ongoing development of the novel analysis methods embedded in more user-friendly commercial and open source software packages (see, e.g., [megcommunity.org](http://megcommunity.org)) will boost the advancement of MEG both in basic brain research and in clinical and pre-clinical studies aiming at new clinical applications.

Exciting development is ongoing in alternative sensor technologies, such as atomic magnetometers and high- $T_c$  SQUIDs. Measurements of good quality MEG signals using configurations of single or few sensors without liquid helium have been reported. Despite the new sensors having exhibited higher noise levels than the low- $T_c$  SQUIDs, they can be placed closer to the scalp and hence increase the SNR of MEG.

### Concluding remarks

Advances in technology, such as the development of zero helium boil-off recycling and advanced hardware- and software-based magnetic shielding methods, have had a significant impact on commercial MEG systems. With the help of such effective ‘software magnetic shielding’ the required hardware shielding, the magnetically shielded room, can be made lighter and cheaper. This kind of technical improvement and development of user-friendly MEG-specific clinical analysis software may be an effective booster for wider adoption of MEG in hospitals.

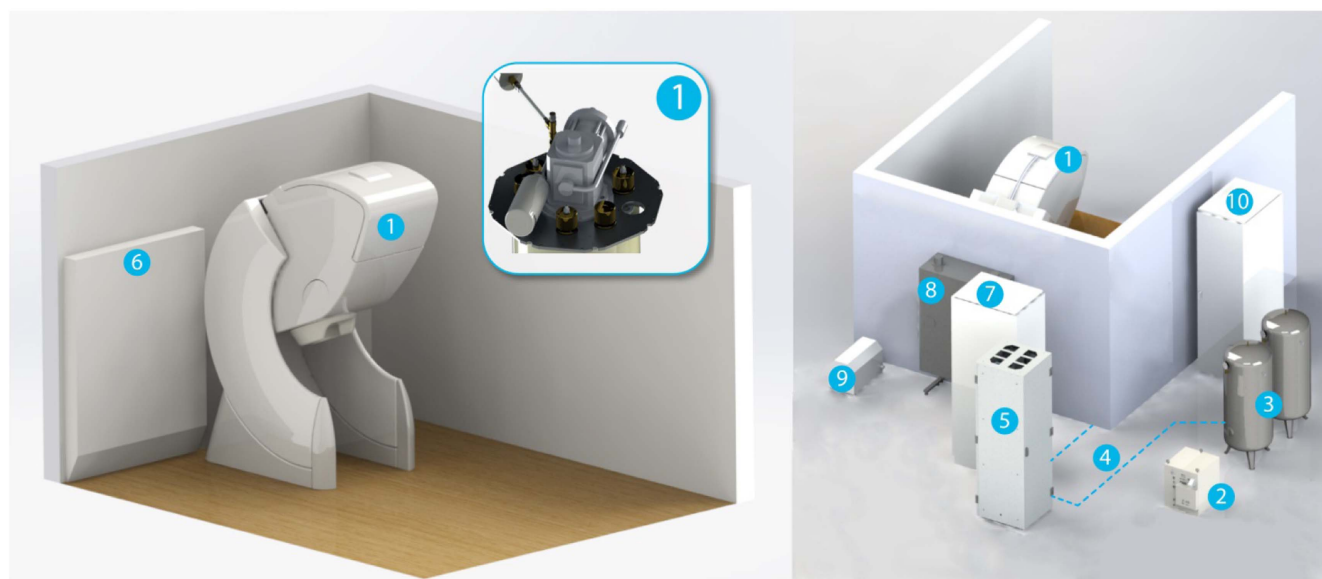


**Figure 17.** Internal helium recycling system (Elekta Oy). (1). Cryocooler cold head is inserted in the top part of the dewar in the MEG probe unit inside the magnetically shielded room. (2). Cryocooler compressor. (3). Storage tanks. (4). Helium gas lines. (5). Helium recycler cabinet. (6). Reel for cryocooler hoses. (7). MEG electronics cabinets. (8). MEG electronics feedthrough unit. (9). Lifting unit for MEG probe. (10). Cabinet for stimulators. Items 1–6 are parts specific to the helium recycler.

Despite the promising development of alternative sensor types (atomic magnetometers and high- $T_c$  SQUIDs), they still need a substantial effort to demonstrate a fully functional whole-head system with more than 100 sensors. Therefore, whole-head MEG systems utilizing low- $T_c$ -SQUIDs, liquid helium recycling and sophisticated interference elimination techniques, are the most practical tools for detecting the brain's magnetic fields today. Development of robust and cheaper sensor technologies may also provide commercially viable systems in other applications, such as magnetic markers in immunoassays (chapter 7) and adult and fetal MCG.

In addition to sensor technologies, new applications such as ULF MRI (chapter 4), development of hybrid systems combining MEG and MRI (chapter 5), and NCI (chapter 6)

are expected to increase the interest and need for biomagnetic functional imaging systems. These new technologies are still at the early research stage and their commercial viability needs to be evaluated.

MEG is currently receiving broader attention, because of emerging new applications and efforts in developing new sensor technologies. Current clinical applications (epilepsy and pre-surgical mapping) can be boosted with better analysis software to ensure sufficient patient throughput in clinics. Potential new applications rely partly on increased sensitivity of MEG, by lowering sensor noise (chapter 1) and/or bringing the sensors close to scalp (chapter 6). The scientific and technological advances can increase the market growth.

## References

- [1] Baule G M and McFee R 1963 Detection of the magnetic field of the heart *Am. Heart J.* **55** 95–6
- [2] Cohen D 1968 Magnetoencephalography: evidence of magnetic fields produced by alpha-rhythm currents *Science* **161** 784–6
- [3] Cohen D, Edelsack E A and Zimmerman J E 1970 Magnetocardiograms taken inside a shielded room with a superconducting point-contact magnetometer *Appl. Phys. Lett.* **16** 278–80
- [4] Cohen D 1972 Magnetoencephalography: detection of brain's electric activity with a superconducting magnetometer *Science* **175** 664–6
- [5] Deaver B S and Fairbank W M 1961 Experimental evidence for quantized flux in superconducting cylinders *Phys. Rev. Lett.* **7** 43–6
- [6] Doll R and Näbauer M 1961 Experimental proof of magnetic flux quantization in a superconducting ring *Phys. Rev. Lett.* **7** 51–2
- [7] Josephson B D 1962 Possible new effects in superconductive tunnelling *Phys. Lett.* **1** 251–3
- [8] Anderson P W and Rowell J M 1963 Probable observation of the Josephson superconducting tunneling effect *Phys. Rev. Lett.* **10** 230–2
- [9] Jaklevic R C, Lambe J, Silver A H and Mercereau J E 1964 Quantum interference effects in Josephson tunneling *Phys. Rev. Lett.* **12** 159–60
- [10] Clarke J and Braginski A I (ed) 2004 *The SQUID Handbook: Fundamentals and Technology of SQUIDS and SQUID Systems* vol I (Weinheim, Germany: Wiley-VCH) (doi:10.1002/3527603646)
- [11] Clarke J and Braginski A I (ed) 2006 *The SQUID Handbook: Applications of SQUIDS and SQUID Systems* vol II (Weinheim, Germany: Wiley-VCH) (doi:10.1002/9783527609956)
- [12] Nenonen J, Montonen J and Katila T 1996 Thermal noise in biomagnetic measurements *Rev. Sci. Instrum.* **67** 2397–405
- [13] Fedele T, Scheer H J, Burghoff M, Curio G and Körber R 2015 Ultra-low-noise EEG/MEG systems enable bimodal non-invasive detection of spike like human somatosensory evoked potentials *Physiol. Meas.* **36** 357–68
- [14] McDermott R, Lee S-K, ten Haken B, Trabesinger A H, Pines A and Clarke J 2004 Microtesla MRI with a superconducting quantum interference device *Proc. Natl Acad. Sci. USA* **101** 7857–61
- [15] Seton H C, Hutchison J M S and Bussell D M 1997 A 4.2 K receiver coil and SQUID amplifier used to improve the SNR of low field magnetic resonance images of the human arm *Meas. Sci. Technol.* **8** 198–207
- [16] Matlashov A N, Burmistrov E, Magnelind P E, Schultz L, Urbaitis A V, Volegov P L, Yoder J and Espy M A 2012 SQUID-based systems for co-registration of ultra-low field nuclear magnetic resonance images and magnetoencephalography *Physica C* **482** 19–26
- [17] Myers W, Slichter D, Hatridge M, Busch S, Mössle M, McDermott R, Trabesinger A and Clarke J 2007 Calculated signal-to-noise ratio of MRI detected with SQUIDS and Faraday detectors in fields from 10 microT to 1.5 T *J. Magn. Reson.* **186** 182–92
- [18] Seton H C, Hutchison J M S and Bussell D M 2005 Liquid helium cryostat for SQUID-based MRI receivers *Cryogenics* **45** 348–55
- [19] Kahn S and Cohen D 2013 Magnetic noise from the inner wall of a magnetically shielded room *Rev. Sci. Instrum.* **84** 056101
- [20] Uusitalo M A and Ilmoniemi R J 1997 Signal space projection method for separating MEG or EEG into components *Med. Biol. Eng. Comput.* **35** 135–40
- [21] Hilschenz I, Körber R, Scheer H-J, Fedele T, Albrecht H-H, Cassarà A M, Hartwig S, Trahms L, Haase J and Burghoff M 2013 Magnetic resonance imaging at frequencies below 1 kHz *Magn. Reson. Imag.* **31** 171–7
- [22] Matlashov A, Magnelind P, Volegov P and Espy M 2015 Elimination of 1/f noise in gradiometer for SQUID-based ultra-low field nuclear magnetic resonance *15th Int. Conf. on Superconductive Electronics (ISEC) (Nagoya, 2015)* pp 1–3
- [23] Anders S, Schmelz M, Fritzsche L, Stolz R, Zakosarenko V, Schönau T and Meyer H-G 2009 Sub-micrometer-sized, cross-type Nb–AlO<sub>x</sub>–Nb tunnel junctions with low parasitic capacitance *Supercond. Sci. Technol.* **22** 064012
- [24] Hwang S-M, Kim K, Yu K K, Lee S-J, Shim J H, Körber R and Burghoff M 2014 Type-I superconductor pick-up coil in superconducting quantum interference device-based ultra-low-field nuclear magnetic resonance *App. Phys. Lett.* **104** 062602
- [25] Hämäläinen M, Hari R, Ilmoniemi R J, Knuutila J and Lounasmaa O V 1993 Magnetoencephalography—theory, instrumentation and applications to noninvasive studies of the working human brain *Rev. Mod. Phys.* **65** 413–97
- [26] Hari R and Salmelin R 2012 Magnetoencephalography: from SQUID to neuroscience *NeuroImage* **61** 386–96
- [27] American Academy of Neurology Professional Association (AANPA) 2009 Magneto-encephalography (MEG) policy. Recommended by the AANPA medical economics and management committee. Approved by the AANPA Board of directors on May 8, St. Paul, MN, AANPA.
- [28] Mäkelä J P, Forss N, Jääskeläinen J, Kirveskari E, Korvenoja A and Paetau R 2006 Magnetoencephalography in neurosurgery *Neurosurgery* **59** 493–510
- [29] Parkkonen L, Andersson J, Hämäläinen M and Hari R 2008 Early visual brain areas reflect the percept of an ambiguous scene *Proc. Natl Acad. Sci. USA* **105** 20500–4
- [30] Zhdanov A, Nurminen J, Baess P, Hirvenkari L, Jousmäki V, Mäkelä J P, Mandel A, Meronen L, Hari R and Parkkonen L 2015 An internet-based real-time audiovisual link for dual MEG recordings *PLoS One* **10** e0128485
- [31] Tesan G, Johnson B W, Reid M, Thornton R and Crain S 2010 Measurement of neuromagnetic brain function in pre-school children with custom-sized MEG *J. Vis. Exp.* e1693
- [32] Taulu S and Simola J 2006 Spatiotemporal signal space separation method for rejecting nearby interference in MEG measurements *Phys. Med. Biol.* **51** 1759–68
- [33] Gross J *et al* 2013 Good practice for conducting and reporting MEG research *NeuroImage* **65** 349–63
- [34] Öijsjöen F, Schneiderman J F, Figueras G A, Chukharkin M L, Kalabukhov A, Hedström A, Elam M and Winkler D 2012 High-Tc superconducting quantum interference device recordings of spontaneous brain activity: towards high-Tc magnetoencephalography *Appl. Phys. Lett.* **100** 132601–4
- [35] Sander T H, Preusser J, Mhaskar R, Kitching J, Trahms L and Knappe S 2012 Magnetoencephalography with a chip-scale atomic magnetometer *Biomed. Opt. Express* **3** 981–90
- [36] Vesanen P T *et al* 2013 Hybrid ultra-low-field MRI and MEG system based on a commercial whole-head neuromagnetometer *Magn. Res. Med.* **69** 1795–804
- [37] Buzaki G and Watson BO 2012 Brain rhythms and neural syntax: implications for efficient coding of cognitive content and neuropsychiatric disease *Dialogues Clin. Neurosci.* **14** 345–67
- [38] Dammers J, Chocholacs H, Eich E, Boers F, Faley M, Dunin-Borkowski R E and Shah N J 2014 Source localization of brain activity using helium-free interferometer *Appl. Phys. Lett.* **104** 213705
- [39] Schneiderman J F 2014 Information content with low-versus high-Tc SQUID arrays in MEG recordings: the case for high-Tc SQUID-based MEG *J. Neurosci. Methods* **222** 42–6



- [40] Faley M I *et al* 2013 High-Tc DC SQUIDs for magnetoencephalography *IEEE Trans. Appl. Supercond.* **23** 1600705
- [41] Chesca B, John D and Mellor C J 2015 Flux-coherent series SQUID array magnetometers operating above 77 K with superior white flux noise than single-SQUIDs at 4.2 K *Appl. Phys. Lett.* **107** 162602
- [42] Faley M I *et al* 2012 Magnetoencephalography using a multilayer high-Tc DC SQUID magnetometer *Phys. Procedia* **36** 66–71
- [43] Arpaia R, Arzeo M, Nawaz S, Charpentier S, Lombardi F and Bauch T 2014 Ultra low noise YBaCuO nano superconducting quantum interference devices implementing nanowires *Appl. Phys. Lett.* **104** 072603
- [44] Brake H J M T, Burger J F, Holland H J and Lerou P P M 2008 Micromachined cryogenic coolers for cooling low-temperature detectors and electronics *IEEE Sensors Conf. (Lecce, 2008)* pp 1352–5
- [45] Koo C, Godley R F, McDougall M P, Wright S M and Han A 2014 A microfluidically cryocooled spiral microcoil with inductive coupling for MR microscopy *IEEE Trans. Biomed. Eng.* **61** 76–84
- [46] Melgaard S D, Albrecht A R, Hehlen M P and Sheik-Bahae M 2016 Solid-state optical refrigeration to sub-100 Kelvin regime *Sci. Rep.* **6** 20380
- [47] McDermott R, Trabesinger A H, Mück M, Hahn E L, Pines A and Clarke J 2002 Liquid-state NMR and scalar couplings in microtesla magnetic fields *Science* **295** 2247–49
- [48] Inglis B, Buckenmaier K, SanGiorgio P, Pedersen A F, Nichols M A and Clarke J 2013 MRI of the human brain at 130 microtesla *P. Natl. Acad. Sci. USA* **110** 19194
- [49] Clarke J, Hatridge M and Mölle M 2007 SQUID-detected magnetic resonance imaging in microtesla fields *Annu Rev Biomed Eng* **9** 389–413
- [50] Bryant R 1996 The dynamics of water-proton interactions *Annu. Rev. Biophys. Biomol. Struct.* **25** 29–53
- [51] Busch S E, Hatridge M, Mölle M, Myers W, Wong T, Mück M, Chew K, Kuchinsky K, Simko J and Clarke J 2012 Measurements of  $T_1$ -relaxation in *ex vivo* prostate tissue at 132  $\mu$ T *Magn. Reson. Med.* **67** 1138–45
- [52] Drung D, Abmann C, Beyer J, Peters M, Ruede F and Schurig T 2007 Highly sensitive and easy-to-use SQUID sensors *IEEE Trans. Appl. Supercond.* **17** 699–704
- [53] Zevenhoven K C J, Dong H, Ilmoniemi R J and Clarke J 2015 Dynamical cancellation of pulse-induced transients in a metallic shielded room for ultra-low-field magnetic resonance imaging *Appl. Phys. Lett.* **106** 034101
- [54] Zotev V S, Matlashov A N, Volegov P L, Savukov I M, Espy M A, Mosher J C, Gomez J J and Kraus R H 2008 Microtesla MRI of the human brain combined with MEG *J. Magn. Reson.* **194** 115–20
- [55] Zotev V S, Volegov P L, Matlashov A N, Espy M A, Mosher J C and Kraus R H Jr 2008 Parallel MRI at microtesla fields *J. Magn. Reson.* **192** 197–208
- [56] Lin F H, Vesanan P T, Nieminen J O, Hsu Y-C, Zevenhoven K C J, Dabek J, Parkkonen L T, Zhdanov A and Ilmoniemi R J 2013 Noise amplification in parallel whole-head ultra-low-field magnetic resonance imaging using 306 detectors *Magn. Reson. Med.* **70** 595–600
- [57] Elektro Neuromag Oy, Helsinki, Finland, <http://elektro.com>
- [58] Volegov P, Matlachov A N, Espy M A, George J S and Kraus R H Jr 2004 Simultaneous magnetoencephalography and SQUID detected nuclear MR in microtesla magnetic fields *Magn. Reson. Med.* **52** 467–70
- [59] Magnelind P E, Gomez J J, Matlashov A N, Owens T, Sandin J H, Volegov P L and Espy M A 2011 Co-registration of interleaved MEG and ULF MRI using a 7 channel low- $T_c$  SQUID system *IEEE Trans. Appl. Supercond.* **21** 456–60
- [60] Nieminen J O, Zevenhoven K C J, Vesanan P T, Hsu Y-C and Ilmoniemi R J 2014 Current-density imaging using ultra-low-field MRI with adiabatic pulses *Magn. Reson. Imaging* **32** 54–9
- [61] Zevenhoven K C J and Alanko S 2014 Ultra-low-noise amplifier for ultra-low-field MRI main field and gradients *J. Phys.: Conf. Ser.* **507** 042050
- [62] Luomahaara J *et al* 2011 All-planar SQUIDs and pickup coils for combined MEG and MRI *Supercond. Sci. Technol.* **24** 075020
- [63] Supek S and Aine C J (ed) 2014 *Magnetoencephalography* (Heidelberg: Springer-Verlag)
- [64] Vesanan P T, Nieminen J O, Zevenhoven K C J, Hsu Y-C and Ilmoniemi R J 2014 Current-density imaging using ultra-low-field MRI with zero-field encoding *Magn. Reson. Med.* **32** 766–70
- [65] Kraus R Jr, Espy R, Magnelind R and Volegov P 2014 Ultra-low field nuclear magnetic resonance *A New MRI Regime* (New York: Oxford University Press)
- [66] Babiloni C, Pizzella V, Gratta C D, Ferretti A and Romani G L 2009 Fundamentals of electroencephalography, magnetoencephalography, and functional magnetic resonance imaging *Int. Rev. Neurobiol.* **86** 67–80
- [67] Goense J B M and Logothetis N K 2008 Neurophysiology of the BOLD fMRI signal in awake monkeys *Curr. Biol.* **18** 631–40
- [68] Hagberg G E, Bianciardi M and Maraviglia B 2006 Challenges for detection of neuronal currents by MRI *Magn. Reson. Imaging* **24** 483–93
- [69] Kraus R H, Volegov P, Matlachov A and Espy M 2008 Toward direct neural current imaging by resonant mechanisms at ultra-low field *NeuroImage* **39** 310–7
- [70] Bandettini P A, Petridou N and Bodurka J 2005 Direct detection of neuronal activity with MRI: fantasy, possibility, or reality? *Appl. Magn. Reson.* **29** 65–88
- [71] Kim K, Lee S J, Kang C S, Hwang S M, Lee Y H and Yu K K 2014 Toward a brain functional connectivity mapping modality by simultaneous imaging of coherent brainwaves *NeuroImage* **91** 63–9
- [72] Körber R, Nieminen J O, Höfner N, Jazbinšek V, Scheer H J, Kim K and Burghoff M 2013 An advanced phantom study assessing the feasibility of neuronal current imaging by ultra-low-field NMR *J. Magn. Reson.* **237** 182–90
- [73] Sims J R, Schilling J B, Swenson C A, Gardner D L, Matlashov A N and Ammermann C N 2010 Low-noise pulsed pre-polarization magnet systems for ultra-low field NMR *IEEE Trans. Appl. Supercond.* **20** 752–5
- [74] Pankhurst Q A *et al* 2009 Progress in applications of magnetic nanoparticles in biomedicine *J. Phys. D: Appl. Phys.* **42** 224001
- [75] Yang S Y *et al* 2013 Clinic applications in assaying ultra-low-concentration bio-markers using HTS SQUID-based AC magnetosusceptometer *IEEE Trans. Appl. Supercond.* **23** 1600604
- [76] Chieh J J *et al* 2015 Dual-imaging model of SQUID biosusceptometry for locating tumors targeted using magnetic nanoparticles *J. Nanobiotechnology* **13** 11
- [77] Huang K W *et al* 2016 Rapid and quantitative discrimination of tumor cells on tissue slices *Nanotechnology* **27** 235101
- [78] Eberbeck D *et al* 2009 Specific binding of magnetic nanoparticle probes to platelets in whole blood detected by magnetorelaxometry *J. Magn. Magn. Mater.* **321** 1617–20
- [79] Hathaway H J *et al* 2011 Detection of breast cancer cells using targeted magnetic nanoparticles and ultra-sensitive magnetic field sensors *Breast Cancer Res.* **13** R108

- [80] Kuma H *et al* 2010 Liquid phase immunoassays utilizing magnetic markers and SQUID magnetometer *Clin. Chem. Lab. Med.* **48** 1263–9
- [81] Enpuku K *et al* 2014 Liquid-phase immunoassay utilizing binding reactions between magnetic markers and targets in the presence of a magnetic field *Appl. Phys. Express* **7** 097001
- [82] Yoshida T *et al* 2013 Characterization of magnetically fractionated magnetic nanoparticles for magnetic particle imaging *J. Appl. Phys.* **114** 173908
- [83] Vrba J, Nenonen J and Trahms L 2006 Biomagnetism *The SQUID Handbook: Applications of SQUIDs and SQUID Systems* vol II ed A Braginski and J Clarke (Weinheim, Germany: Wiley-VCH) **ch 11**
- [84] Knuutila J, Ahonen A, Hämäläinen M, Kajola M, Laine P, Lounasmaa O, Parkkonen L, Simola J and Tesche C 1993 A 122-channel whole-cortex SQUID system for measuring the brain's magnetic fields *IEEE Trans. Mag.* **29** 3315–2
- [85] Kominis I, Kornack T, Allred J and Romalis M 2003 A subfemtotesla multichannel atomic magnetometer *Nat. London* **422** 596
- [86] Pannetier M, Fermon C, Goff G, Simola J and Kerr E 2004 Femtotesla magnetic field measurement with magnetoresistive sensors *Science* **304** 1648–50
- [87] Taulu S, Simola J, Nenonen J and Parkkonen L 2014 Novel noise reduction methods *Magnetoencephalography* ed S Supek and C J Aine (Berlin: Springer) pp 35–71
- [88] Kiviranta M, Grönberg L and Hassel J 2012 A Multiloop SQUID and a SQUID array with 1  $\mu\text{m}$  and submicrometer input coils *IEEE Trans. Appl. Supercond.* **22** 1600105
- [89] Taulu S and Kajola M 2005 Presentation of electromagnetic multichannel data: the signal space separation method *J. Appl. Phys.* **97** 1–10
- [90] Jin K, Alexopoulos A, Mosher J and Burgess R 2013 Implanted medical devices or other strong sources of interference are not barriers to magnetoencephalographic recordings in epilepsy patients *Clin. Neurophysiol.* **124** 1283–9